NASA TN D-596

TECHNICAL NOTE

D-596

GYROSCOPIC MOTION

OF AN UNSYMMETRICAL SATELLITE

UNDER NO EXTERNAL FORCES

By Manfred E. Kuebler

George C. Marshall Space Flight Center
Huntsville, Alabama

NATIONAL AERONAUTICS AND SPACE ADMINISTRATION

WASHINGTON

December 1960

TABLE OF CONTENTS

LIST OF ILLUSTRATIONS

LIST OF SYMBOLS

A, B, C	Maximum, mean and minimum moment of inertia. Also, the three corresponding body axes
a, b, c	Amplitudes of the angular velocities of the satellite
e	Index for end condition
G	Angular momentum
$\vec{I}$	Instantaneous angular velocity vector
K	Complete elliptic integral
k, k	Moduli of elliptic integrals
$\vec{L}$	Angular momentum vector
O	Center of inertia ellipsoid
p	Distance of O from fixed plane on which ellipsoid is rolling
T	Double of kinetic energy
ΔT	Energy difference
T_0, T_e	Initial and end energy
t	Time
v	Velocity
x, y, z	Axes of inertia ellipsoid
α, β, γ	Directional cosines
δ	Nutation frequency
η	Unsymmetry ratio
λ, μ, ν	Directional cosines
ρ	Rod ratio
τ	Arbitrary time constant
ω_A, ω_B, ω_C	Angular velocities in body fixed coordinates
Ω	Initial angular velocity about axis of minimum moment of inertia, also called true spin
ω_e	Final angular velocity about axis of maximum moment of inertia, also called flat spin

LIST OF ILLUSTRATIONS (Continued)

NATIONAL AERONAUTICS AND SPACE ADMINISTRATION

TECHNICAL NOTE D-596

GYROSCOPIC MOTION OF AN UNSYMMETRICAL SATELLITE UNDER NO EXTERNAL FORCES

by: Manfred E. Kuebler

Work on this project was completed July 5, 1960.

SUMMARY

This report gives the results of an investigation on the transition from spin about the axis of minimum moment of inertia to spin about the axis of maximum moment of inertia by dissipation of internal mechanical energy. A mathematical discussion, together with charts and diagrams, shows that angular velocities and nutation angle are dependent on the energy and symmetry factors. The low stability of rotation about the axis of maximum moment of inertia, when this inertia is only slightly greater than the mean moment of inertia, is shown.

Section I. INTRODUCTION

Theory and practical experience from orbiting satellites have shown that the rotation of a satellite about its axis of minimum moment of inertia is unstable. This instability is caused by the incomplete rigidity of a satellite and dissipation of mechanical energy by internal friction of the body. The body begins to nutate with increasing angle. Finally the satellite rotates about its axis of maximum moment of inertia. This motion is stable. The final spin is slower than the initial spin. The angular momentum stays constant during the transition.

It has been suggested that this natural behavior of a rod-shaped body spinning about its axis of minimum moment of inertia be applied to spin reduction purposes (Satellite S-15). In this connection the time within which the transition takes place and the degree of stability of the spin about the axis of maximum moment of inertia are important.

This report gives the results of a study of the motion of the body at any energy level. The angular velocities of the nutational motion are presented as dependent on the energy and the unsymmetry factors of the satellite. The nutational path of the axis of maximum moment of inertia of the body as seen by a space fixed observer is shown.

Section II. MOTION OF SATELLITE IN BODY FIXED COORDINATES

Consider the satellite as an unsymmetrical top with three different principal moments of inertia $A > B > C$. C is the moment of inertia around the original spin axis or longitudinal axis of the body.

If ω_A, ω_B, ω_C are the angular velocities around the corresponding axes of principal moments of inertia, the Eulerian equations read:

$$\begin{aligned} A\dot{\omega}_A - (B - C)\,\omega_B\omega_C &= 0 \\ B\dot{\omega}_B - (C - A)\,\omega_C\omega_A &= 0 \\ C\dot{\omega}_C - (A - B)\,\omega_A\omega_B &= 0 \end{aligned} \tag{1}$$

A first integral of these equations is

$$A\omega_A^2 + B\omega_B^2 + C\omega_C^2 = T \tag{2}$$

where T is a constant and represents the double of the kinetic energy of the moving body.

A second integral is obtained by multiplying Equations 1 by $A\omega_A$, $B\omega_B$, $C\omega_C$, respectively, adding and integrating

$$A^2\omega_A^2 + B^2\omega_B^2 + C^2\omega_C^2 = G^2 \tag{3}$$

This is the square of the total angular momentum. Initially, during true spin about the longitudinal axis with $\omega_C = \Omega$ and $\omega_A = \omega_B = 0$

$$G^2 = C^2\Omega^2 \tag{4}$$

and

$$T_0 = C\,\Omega^2 \tag{5}$$

During the transition period, G will remain constant while T will be continuously decreasing, due to the dissipation of mechanical energy. Finally, the body will have flat spin at the angular velocity

$$\omega_{A_e} = \frac{C}{A}\Omega \quad \text{and} \quad \omega_{B_e} = \omega_{C_e} = 0 \tag{6}$$

The angular momentum will stay constant at $G = C\,\Omega = A\omega_{A_e}$ and the kinetic energy will be decreased to the value

$$T_e = A\omega_A^2 = \frac{C}{A}\,C\,\Omega^2 = \frac{C}{A}T_0 \tag{7}$$

The motion during the transition period is described by Kirchhoff's solution of the unsymmetrical top. In terms of elliptic doubly periodic functions for

$$BT > G^2 \tag{8}$$

$$\begin{aligned} \omega_A &= c \cdot \operatorname{cn} \delta(t-\tau) \\ \omega_B &= b \cdot \operatorname{sn} \delta(t-\tau) \\ \omega_C &= a \cdot \operatorname{dn} \delta(t-\tau) \end{aligned} \tag{9}$$

where

$$a^2 = \frac{AT - G^2}{C(A-C)} \qquad b^2 = \frac{G^2 - CT}{B(B-C)} \qquad c^2 = \frac{G^2 - CT}{A(A-C)}$$

$$\delta^2 = \frac{(B-C)(AT-G^2)}{ABC} \tag{10}$$

$$k^2 = \frac{A-B}{B-C}\,\frac{G^2-CT}{AT-G^2} < 1$$

For the energy range of $\frac{G^2}{C} > T > \frac{G^2}{B}$ this means that the body oscillates about the A and B axes with maximum angular velocities c and b. The A and B axes vary approximately as cosine and sine $[\lambda(t-\tau)]$, respectively. The motion about the body fixed C axis is a rotation of angular velocity always fluctuating in the same direction. The periods of the oscillations are given by the complete elliptic integral and are equal to $\frac{4K(k)}{\delta}$. For the fluctuating angular velocity the period is $\frac{2K(k)}{\delta}$. After more and more energy is dissipated, the motion reaches the state where

$$BT = G^2 \tag{11}$$

Then $k = 1$ and the elliptic functions become exponential

$$\begin{aligned} \omega_A &= \frac{a}{\cosh \delta(t-\tau)} \\ \omega_B &= b \tanh \delta(t-\tau) \\ \omega_C &= \frac{c}{\cosh \delta(t-\tau)} \end{aligned} \tag{12}$$

where

$$a^2 = \frac{\left(1-\frac{C}{B}\right)G^2}{A(A-C)} \qquad b^2 = \frac{G^2}{B^2} \qquad c^2 = \frac{\left(\frac{A}{B}-1\right)G^2}{C(A-C)}$$

$$\delta^2 = \frac{\left(A-B\right)\left(1-\frac{C}{B}\right)}{ABC}G^2 \tag{13}$$

Now it is $\lim_{t\to\infty} \frac{1}{\cosh \delta t} = 0$ and $\lim_{t\to\infty} \tanh \delta t = 1$ so that for $t \to \infty$ $\omega_1 \to 0$ $\omega_3 \to 0$ $\omega_2 \to \frac{G}{B} = \frac{C}{B}\Omega$. This means that if the energy T would remain on the magnitude $T = \frac{G^2}{B}$ the body would finally settle on a rotation about its axis of mean moment of inertia. However, since this motion is not gained instantly after arrival at $T = \frac{G^2}{B}$, energy is still dissipated by the irregular motion. The body enters the phase where

$$G^2 > BT \tag{14}$$

The solution of Euler's equations for this range is

$$\begin{aligned} \omega_A &= a \operatorname{dn} \delta(t-\tau) \\ \omega_B &= b \operatorname{sn} \delta(t-\tau) \\ \omega_C &= c \operatorname{cn} \delta(t-\tau) \end{aligned} \tag{15}$$

where

$$a^2 = \frac{G^2 - CT}{A(A-C)} \qquad b^2 = \frac{AT - G^2}{B(A-B)} \qquad c^2 = \frac{AT - G^2}{C(A-C)}$$

$$\delta^2 = \frac{(A-B)(G^2-CT)}{ABC} \tag{16}$$

$$k^2 = \frac{B-C}{A-B} \cdot \frac{AT-G^2}{G^2-CT} < 1$$

The energy is now $\frac{G^2}{B} > T > \frac{G^2}{A}$. The essential change in the motion compared with the phase $\frac{G^2}{C} > T > \frac{G^2}{B}$ is that the motion about the B and C axes is of oscillatory type, while the body rotates about the A axis with angular velocity fluctuating in the same direction always.

The part of the investigation which describes the motion in body fixed coordinates is especially suited for the design of a nutation damper.

Section III. MOTION OF SATELLITE AS SEEN BY A SPACE FIXED OBSERVER

In using Poinsot's construction, it is assumed that for a finite time interval kinetic energy and angular momentum remain constant. This is certainly not true for the energy, but this step-by-step consideration helps explain the motion considerably.

The satellite is replaced by its momental ellipsoid which is defined by the equation

$$Ax^2 + By^2 + Cz^2 = T \tag{17}$$

The x, y, z axes are coinciding with the A, B, C axes of the satellite, respectively. The ellipsoid has the semiaxes $\sqrt{T/A}$; $\sqrt{T/B}$ and $\sqrt{T/C}$ along x, y, z direction, respectively. The momental ellipsoid with a fixed center rolls on a fixed plane at a distance

$$p = \frac{T}{G} \tag{18}$$

from the center of the ellipsoid. The perpendicular from O to the fixed plane points in the direction of the total angular momentum vector and is constant in length if T is kept constant (Fig. 1).

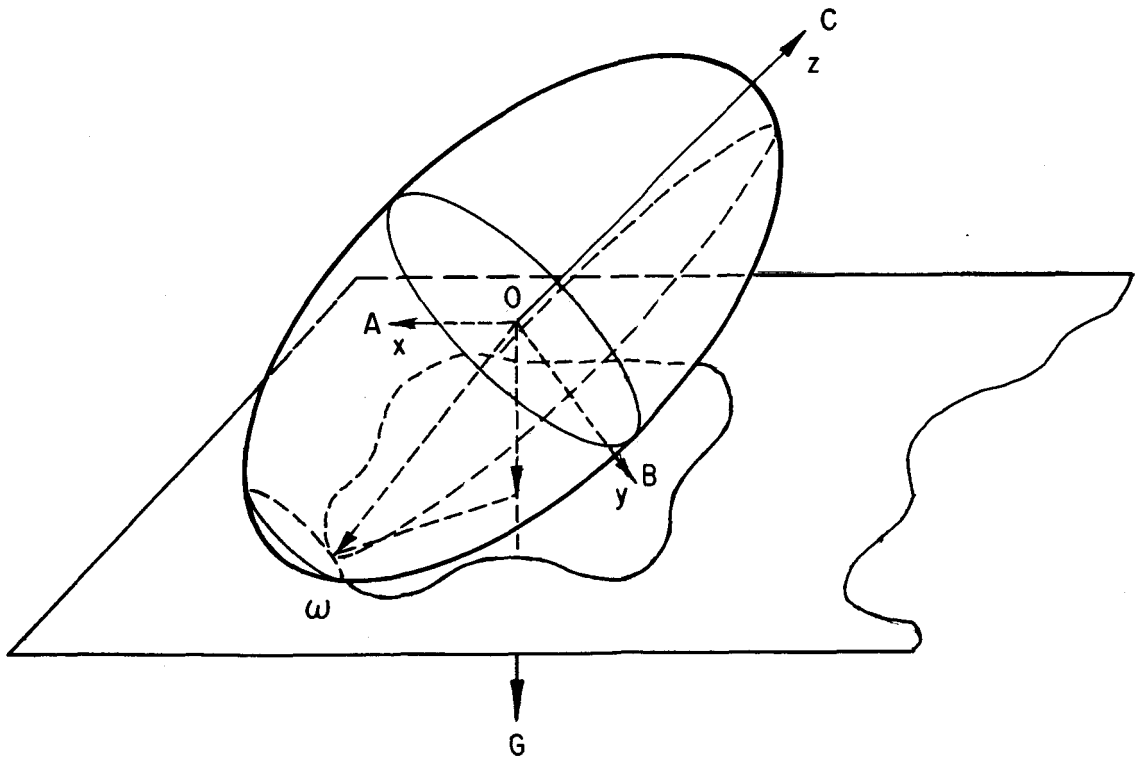

Fig. 1 MOMENTAL ELLIPSOID ROLLING ON FIXED PLANE

The radius vector from the center of the ellipsoid to the contact point with the tangential plane is the instantaneous angular velocity vector, $\vec{\omega}$. As the ellipsoid rolls on the fixed plane the points of contact form a curve on this plane, the herpolhode, and another curve on the ellipsoid, the polhode. Connecting all points of polhode and herpolhode by straight lines with the center O, the motion also can be considered as the rolling of the polhode cone on the herpolhode cone. The polhode cone will be a closed cone while, in general, the herpolhode cone will not be re-entering.

$BT > G^2$ and $BT < G^2$ are to be considered. For the description of the motion in space fixed coordinates the angular momentum vector is chosen as reference line. During the first phase of the transition period with $BT > G^2$, we use the C axis (original spin axis) as body fixed reference line. During the second phase where $BT < G^2$, the A axis is used as body reference line.

$BT > G^2$

Describe a sphere with radius 1 around the center O of the body. The principal axes intersect with this sphere at A, B, C; the angular momentum vector intersects at L. The directional cosines against the space fixed angular momentum vector OL are α, β, γ. λ, μ, ν are angles of the planes LOA, LOB, LOC against some fixed plane LOX passing through OL (Fig. 2). $\frac{d\nu}{dt}$ is the angular velocity of nutation and γ is the nutation angle. The velocity around the instantaneous axis OL is ω which lets C move perpendicular to the arc IC with $v_{IC} = \omega \sin IC$ which yields, resolved perpendicular to LC, a velocity $v_{LC} = \omega \sin IC \sin LCI$. But it is also $v_{LC} = \frac{d\gamma}{dt} \sin \gamma$, therefore by cosine law of spherical trigonometry

$$\sin \gamma \frac{d\nu}{dt} = \omega \sin CI \sin LCI$$

$$= \omega \frac{\cos LI - \cos LC \cos IC}{\sin LC} \qquad (19)$$

$\omega \cos LI$ is the resolved part of the angular velocity about OL which is equal to $\frac{T}{G}$ as seen by the momental ellipsoid. In the same way we find $\omega \cos IC = \omega_C$ so that

$$\sin^2 \gamma \frac{d\nu}{dt} = \frac{T}{G} - \omega_C \cos \gamma \qquad (20)$$

With $G \cos \gamma = C\omega_C$ it follows that

$$\sin^2 \gamma \frac{d\nu}{dt} = \frac{T}{G} - \frac{G \cos^2 \gamma}{C} \qquad (21)$$

or

$$\boxed{\frac{d\nu}{dt} = \frac{T}{G} + \frac{CT - G^2}{CG} \operatorname{ctg}^2 \gamma} \qquad (22)$$

For determination of $\frac{d\alpha}{dt}$, the directional cosines of the angular momentum line OL can be expressed as

$$\cos \alpha = \frac{A\omega_A}{G} \qquad \cos \beta = \frac{B\omega_B}{G} \qquad \cos \gamma = \frac{C\omega_C}{G}$$

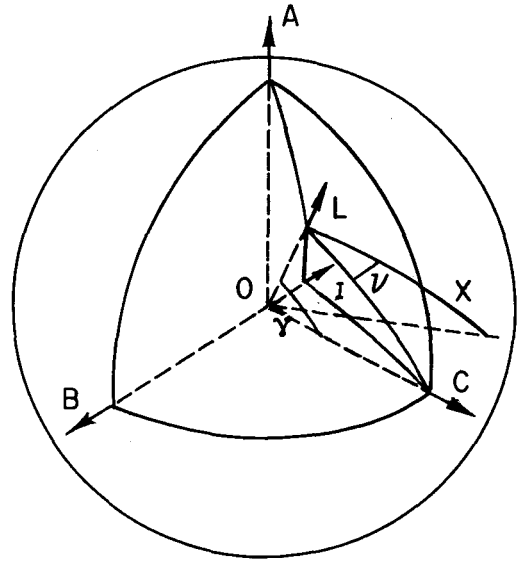

Fig. 2 UNIT SPHERE SHOWING GEOMETRY OF MOVING AXES -- $BT > G^2$

Substituting into Euler's equation

$$C\frac{d\omega_C}{dt} - (A-B)\omega_A\omega_B = 0 \qquad (23)$$

it follows that

$$\sin\gamma\frac{d\gamma}{dt} = \left(\frac{1}{A}-\frac{1}{B}\right)\cos\alpha\ \cos\beta\cdot G \qquad (24)$$

Because of the relations

$$\frac{\cos^2\alpha}{A}+\frac{\cos^2\beta}{B}+\frac{\cos^2\gamma}{C}=\frac{T}{G^2} \qquad (25)$$

$$\cos^2\alpha+\cos^2\beta+\cos^2\gamma=1$$

after elimination of α and β, it becomes

$$\sin^2\gamma\left(\frac{d\gamma}{dt}\right)^2 = -\frac{G^2}{AB}\left[\frac{AT-G^2}{G^2}-\frac{A-C}{C}\cos^2\gamma\right] \times\left[\frac{BT-G^2}{G^2}-\frac{B-C}{C}\cos^2\gamma\right] \qquad (26)$$

In order for the equation to give real values for $\frac{d\gamma}{dt}$, the expressions in brackets must have opposite signs. This leads to the condition

$$\frac{AT-G^2}{G^2}\frac{C}{A-C} > \cos^2\gamma > \frac{BT-G^2}{G^2}\frac{C}{B-C} \qquad (27)$$

By integrating Equations 22 and 26 and plotting γ versus ν, we obtain the figure which the C axis describes in space. γ stays between the two limits as given by Equation 27.

$$\underline{BT < G^2}$$

The procedure is analogous to the previous case for $BT > G^2$. From Figure 3 we find

$$\sin\alpha\frac{d\lambda}{dt} = \omega\sin AI\cos LAI = \omega\frac{\cos LI-\cos LA\cos IA}{\sin LA} \qquad (28)$$

and after short calculation

$$\frac{d\lambda}{dt} = \frac{T}{G}+\frac{AT-G^2}{AG}\cot^2\alpha \qquad (29)$$

Also, the first of Euler's equations shows

$$\sin^2\alpha\left(\frac{d\alpha}{dt}\right)^2 = -\frac{G^2}{BC}\left(\frac{G^2-CT}{G^2}-\frac{A-C}{A}\cos^2\alpha\right) \times\left(\frac{G^2-BT}{G^2}-\frac{A-B}{A}\cos^2\alpha\right) \qquad (30)$$

with the condition

$$\frac{G^2-CT}{G^2}\frac{A}{A-C} > \cos^2\alpha > \frac{G^2-BT}{G^2}\frac{A}{A-B} \qquad (31)$$

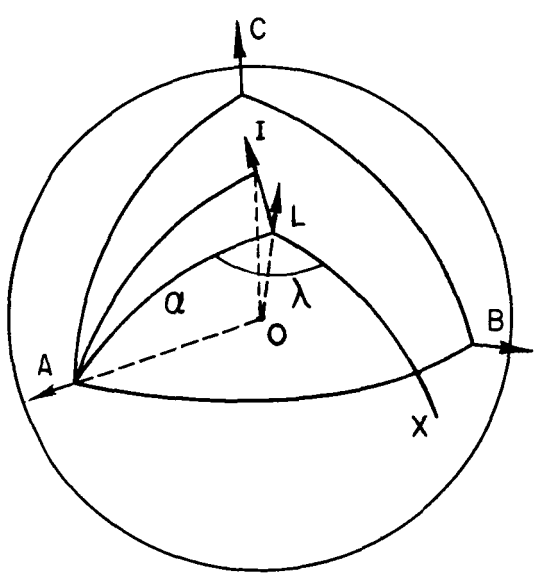

Fig. 3 UNIT SPHERE SHOWING GEOMETRY OF MOVING AXES -- $BT < G^2$

Section IV. NUMERICAL EVALUATION OF THE THEORY OF MOTION

1. Body Fixed Coordinates

$$\frac{G^2}{C} > T > \frac{G^2}{B} \quad \text{or} \quad 0 < \frac{\Delta T}{T_0} < 1 - \frac{C}{B}$$

The amplitudes of ω_A, ω_B, ω_C are calculated in dimensionless form using equations

$$\left(\frac{a}{\Omega}\right)^2 = 1 - \frac{\rho}{\rho - 1}\,\frac{\Delta T}{T_0}$$

$$\left(\frac{b}{\Omega}\right)^2 = \frac{1}{\eta\rho(\eta\rho - 1)}\,\frac{\Delta T}{T_0}$$

$$\left(\frac{c}{\Omega}\right)^2 = \frac{1}{\rho(\rho - 1)}\,\frac{\Delta T}{T_0}$$

$$\left(\frac{\delta}{\Omega}\right)^2 = \left(1 - \frac{1}{\eta\rho}\right)\left(1 - \frac{1}{\rho} - \frac{\Delta T}{T_0}\right)$$

$$k^2 = \frac{1 - \eta}{\eta - 1/\rho}\,\frac{\Delta T/T_0}{\rho(1 - \Delta T/T_0) - 1}$$

$$K = K(k)$$

where

Ω is the initial spin velocity about the C axis

$\eta = \frac{B}{A}$ is the unsymmetry ratio of the body

ΔT is the amount of energy dissipated from the initial energy T_0

K is the complete elliptic integral

$\rho = \frac{A}{C}$ is the rod ratio.

Considering the differential equations for the elliptic functions

$$\left(\frac{d\ sn\ u}{du}\right)^2 = (1 - sn^2\ u)(1 - k^2\ sn^2\ u)$$

$$\left(\frac{d\ cn\ u}{du}\right) = (1 - cn^2\ u)(k'^2 + k^2\ c^2)$$

$$\left(\frac{d\ dn\ u}{du}\right) = (1 - dn^2\ u)(dn^2\ u - k'^2)$$

$$u = \delta t$$

and from tables of elliptic functions, it follows that sn u and dn u oscillate between +1 and −1 at the period 4K, while dn u fluctuates between +1 and +k′ at the period 2K. ω_A and ω_B oscillate with period $\frac{4K}{\delta}$ and ω_C fluctuates with period $\frac{2K}{\delta}$ since $u = \delta \cdot t$.

Figure 4 shows the functions $\frac{a}{\Omega}$ and $\frac{a}{\Omega} \cdot k'$ plotted versus $\frac{\Delta T}{T_0}$. They represent the maxima and minima between which the angular velocity ratio $\frac{\omega_C}{\Omega}$ fluctuates. The curve for the upper limit of $\frac{\omega_C}{\Omega}$ is independent of the unsymmetry factor η. The lower limit depends on η. For $\eta = 1$, for the symmetrical top, upper and lower limits coincide and the angular velocity around the longitudinal axis (axis of symmetry) is constant for a fixed energy level. For the considered η range, $\left(\frac{\omega_C}{\Omega}\right)_{max}$ and $\left(\frac{\omega_C}{\Omega}\right)_{min}$ are represented by the same curve within the drawing accuracy.

The amplitudes $\frac{b}{\Omega}$ and $\frac{c}{\Omega}$ of the angular velocity ratios $\frac{\omega_B}{\Omega}$ and $\frac{\omega_A}{\Omega}$ are plotted versus

$\frac{\Delta T}{T_0}$ in Figures 5 and 6. $\frac{b}{\Omega}$ depends on the unsymmetry factor η, while $\frac{c}{\Omega}$ does not. For the symmetrical top with $\eta = 1$, $\frac{b}{\Omega}$ and $\frac{c}{\Omega}$ are equal. This means that the unsymmetry of a gyro influences mainly the motion around the axis of mean moment of inertia. This disturbance causes the fluctuation in the angular velocity around the longitudinal axis.

In Figure 7 the frequency ratio $\frac{\delta/4K}{\Omega/2\pi}$ of the oscillatory angular velocities ω_A and ω_B is plotted versus $\frac{\Delta T}{T_0}$. The frequency depends on η, however in the range of unsymmetry considered, it does not appear. The frequency ratio of the fluctuation of ω_C is twice the values shown in the curve.

$$\frac{G^2}{B} > T > \frac{G^2}{A} \quad \text{or} \quad \frac{1}{\eta} - 1 > \frac{\Delta T^*}{T_e} > 0$$

The diagrams for this range will show the motion of the body as it approaches the flat spin at the energy minimum T_e. Therefore, it is advantageous to make the angular velocities and frequency ratio dimensionless by division through the flat spin velocity $\omega_{A_e} = \omega_e$. ΔT^* is the rest energy which still must be taken out before the body enters flat spin at the energy $T_e = \frac{C}{A} T_0$. The formulas used for presentation in the diagrams are

$$\left(\frac{a^*}{\omega_e}\right)^2 = \frac{\rho - 1 - \Delta T^*/T_e}{\rho - 1}$$

$$\left(\frac{b^*}{\omega_e}\right)^2 = \frac{\Delta T^*/T_e}{\eta(1-\eta)}$$

$$\left(\frac{c^*}{\omega_e}\right)^2 = \frac{(\Delta T^*/T_e)\rho^2}{\rho - 1}$$

$$\left(\frac{\delta^*}{\omega_e}\right)^2 = \left(\frac{1}{\eta} - 1\right)\left(\rho - 1 - \frac{\Delta T^*}{T_e}\right)$$

$$k^{*2} = \frac{\eta - 1/\rho}{1-\eta} \frac{\Delta T^*/T_e}{1 - 1/\rho(1+\Delta T^*/T_e)} = 1 - k^{*\prime 2}$$

$$K^* = K^*(k^*)$$

The upper and lower limits $\frac{a^*}{\omega_e}$ and $\frac{a^*}{\omega_e} \cdot k^{*\prime}$ of the fluctuating angular velocity ratio $\frac{\omega_A}{\omega_e}$ around the axis of maximum moment of inertia are plotted versus $\frac{\Delta T^*}{T_e}$ in Figure 8. The upper limit is independent on the unsymmetry factor η and almost constant over $\frac{\Delta T^*}{T_e}$. (A blown-up diagram is given in Figure 8a.) The lower limit depends on η and coincides with the upper limit for $\eta = \frac{1}{\rho}$ which means symmetry around the A axis. However, the diagrams are designed for the other end of the η range describing a body closer to symmetry around the C axis. (This does not restrict the generality of the problem.) For $\eta = 1$ the equations lose their sense because no lateral axis of the body is preferred about which the final flat spin could take place. This case is already excluded by the definition of the energy range $\frac{1}{\eta} - 1 > \frac{\Delta T^*}{T_e} > 0$.

Figure 9 gives the ratio of the angular velocity about the axis of mean moment of inertia to the final spin rate as function of $\frac{\Delta T^*}{T_e}$. It is strongly influenced by the unsymmetry factor η.

The angular velocity around the axis of smallest moment of inertia is not influenced by η. $\frac{c^*}{\omega_e}$ is plotted versus $\frac{\Delta T^*}{T_e}$ in Figure 10. Figure 11 shows the frequency of the oscillatory angular velocities ω_B^* and ω_C^* in the dimensionless form $\frac{\delta^*/4K}{\omega_e/2\pi}$. This frequency ratio is influenced by $\frac{\Delta T^*}{T_e}$ and η.

2. Space Fixed Coordinates

$$\frac{G^2}{C} > T > \frac{G^2}{B} \quad \text{or} \quad 0 < \frac{\Delta T}{T_0} < 1 - \frac{C}{B}$$

The motion is described by the nutation angle γ of the longitudinal axis of the body (C-axis) against the space fixed angular momentum vector, and the angle ν between the body fixed plane containing the C axis and the angular momentum vector, and some space fixed plane through the angular momentum vector.

The nutation angle γ varies between a maximum and a minimum value which are given by

$$\gamma_{max} = \sin^{-1} \sqrt{\frac{1}{1 - 1/\rho} \frac{\Delta T}{T_0}}$$

and

$$\gamma_{min} = \sin^{-1} \sqrt{\frac{1}{1 - 1/\eta\rho} \frac{\Delta T}{T_0}}$$

Evaluation of these formulas shows, however, that for the range of unsymmetry factors considered in this report γ_{max} and γ_{min} are alike within the accuracy of the diagrams. Therefore only one diagram is given for γ as a function of $\frac{\Delta T}{T_0}$ (Fig. 12). This means that a rather small unsymmetry does not show up in the nutation of the body.

$$\frac{G^2}{B} > T > \frac{G^2}{A} \quad \text{or} \quad \frac{1}{\eta} - 1 > \frac{\Delta T^*}{T_e} > 0$$

The motion is described by the nutation angle α of the axis A of maximum moment of inertia against the angular momentum vector, and the angle λ between the body fixed plane through the A axis and the angular momentum vector and some space fixed plane through the angular momentum vector.

The nutation angle varies between

$$\alpha_{max} = \sin^{-1} \sqrt{\frac{1}{1/\eta - 1} \frac{\Delta T^*}{T_e}}$$

and

$$\alpha_{min} = \sin^{-1} \sqrt{\frac{1}{\rho - 1} \frac{\Delta T^*}{T_e}}$$

which are plotted versus $\frac{\Delta T^*}{T_e}$ in Figures 13 and 13a. The maximum of α is strongly influenced by η and, in contrast to the energy range considered before, there is an essential difference between α_{max} and α_{min}. This is understandable if one considers the body in flat spin as a disk-shaped body with a very large unsymmetry. For better illustration, the nutation angle α is plotted as radius in a polar coordinate system with λ as pole angle. The formulas are

$$\begin{cases} \frac{d\alpha}{dt} = \omega_e \sqrt{\left[\rho - 1 - \frac{1}{\sin^2 \alpha} \frac{\Delta T^*}{T_e}\right]\left[\frac{\Delta T^*}{T_e} - \sin^2 \alpha \left(\frac{1}{\eta} - 1\right)\right]} \\ \frac{d\lambda}{dt} = \omega_e \left[1 + \frac{\Delta T^*}{T_e} + \frac{\Delta T^*}{T_e} \cot^2 \alpha\right] \end{cases}$$

or

$$d\lambda = \frac{\left[1 + \frac{\Delta T^*}{T_e} + \frac{\Delta T^*}{T_e} \cot^2 \alpha\right]}{\sqrt{\left[\rho - 1 - \frac{1}{\sin^2 \alpha} \frac{\Delta T^*}{T_e}\right]\left[\frac{\Delta T^*}{T_e} - \sin^2 \alpha \left(\frac{1}{\eta} - 1\right)\right]}} d\alpha$$

The resulting curves are plotted in Figures 14 and 15. In general, the plots are rose-like figures with an infinite number of leaves. For the range $\frac{G^2}{C} > T > \frac{G^2}{B}$ the corresponding figures of γ versus ν would be circles within the accuracy of the drawing. The evaluation of the theory for the special range of η and a rod ratio of $\rho = 50$ is due to the configuration of satellite S-15 for which this investigation has been made. In order to obtain a somewhat broader view of the problem, additional calculations have been carried out for $\rho = 10$, 20, 30, and 40 and a fixed $\eta = 0.995$. The results are presented in Figures 16 through 23. Functions which are not shown in diagrams are not influenced by ρ.

Section V. CONCLUSIONS

Experience shows that the spin of any satellite at injection into orbit is superimposed by a nutation. This nutation has a body fixed frequency of the same order as the spin. The intense motion causes continuous changes in body strains. Internal friction in turn causes the dissipation of energy. While energy is dissipated the body frequency decreases and the nutation angle increases. The motion of the body is quite intense during the first phase of the transition. No special energy dissipator appears to be necessary.

In the second phase of the transition the body fixed nutation frequency continues to decrease due to energy dissipation. However, the nutation angle and the body fixed angular velocities decrease also. This means a motion connected with fewer and fewer strains to the body. Finally, the body will not be deformed at all and the motion will freeze with a certain rest nutation.

To prevent this and to shorten the time for nutation damping, the use of a nutation damper is necessary. It is suggested that a viscous damper be applied. The driving forces available are: (a) the varying centrifugal force in longitudinal direction of the body and (b) the angular inertia force due to the rocking motion about the longitudinal axis.

For increased efficiency of such a damper it is advisable to use the natural frequency of the motion and design the damper as a resonant system. In this connection the driving force (a) is less favorable because this force oscillates with small amplitudes about a relatively large mean value. The driving force (b) oscillates about zero. The most efficient nutation damper, therefore, seems to be one which makes rotatory oscillations about the longitudinal axis of the satellite with a natural frequency the same as the nutational frequency for $\frac{\Delta T^*}{T_e} = 0$.

The diagrams for the nutation angle as function of the energy surplus show clearly the low stability of the body motion about the axis with a major moment of inertia which is only slightly larger than the mean moment of inertia. A very small disturbance which adds mechanical energy to the body already results in appreciable nutation angles. It is questionable whether the nutation damper is efficient enough to dissipate energies as they may be imparted to the system. However, a final statement cannot be made before a thorough test program has proved the capability of the nutation damper. Modification of the instrumentation for S-15 which permits evaluation of the measurements also under nutation seems to be advisable.

REFERENCE

E. J. Routh, *The Advanced Part of a Treatise on the Dynamics of a System of Rigid Bodies*, Sixth Edition, Dover Publications, Inc., New York.

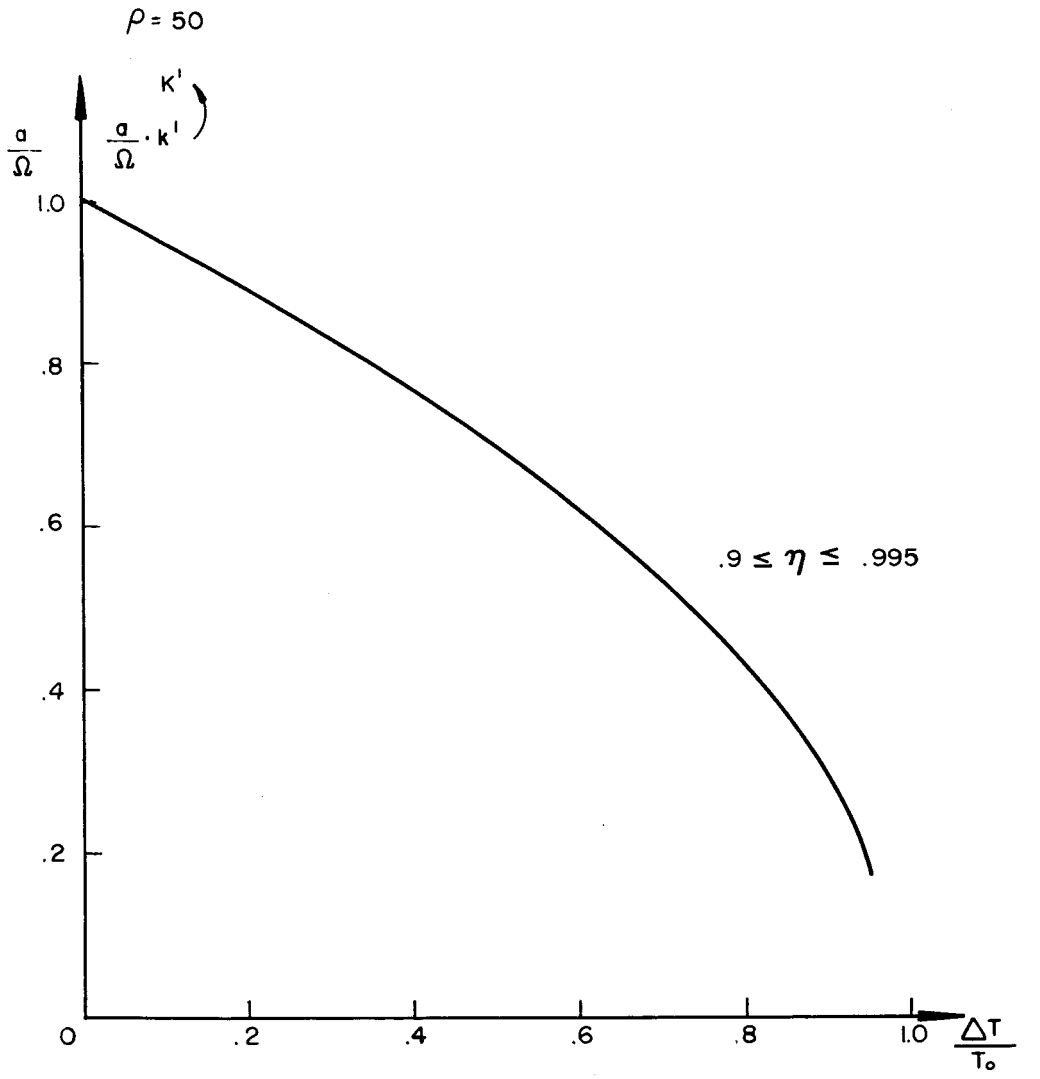

FIG. 4 RATIO OF AMPLITUDE OF SPIN ABOUT THE C AXIS TO THE TRUE SPIN VERSUS ENERGY DISSIPATION RATIO

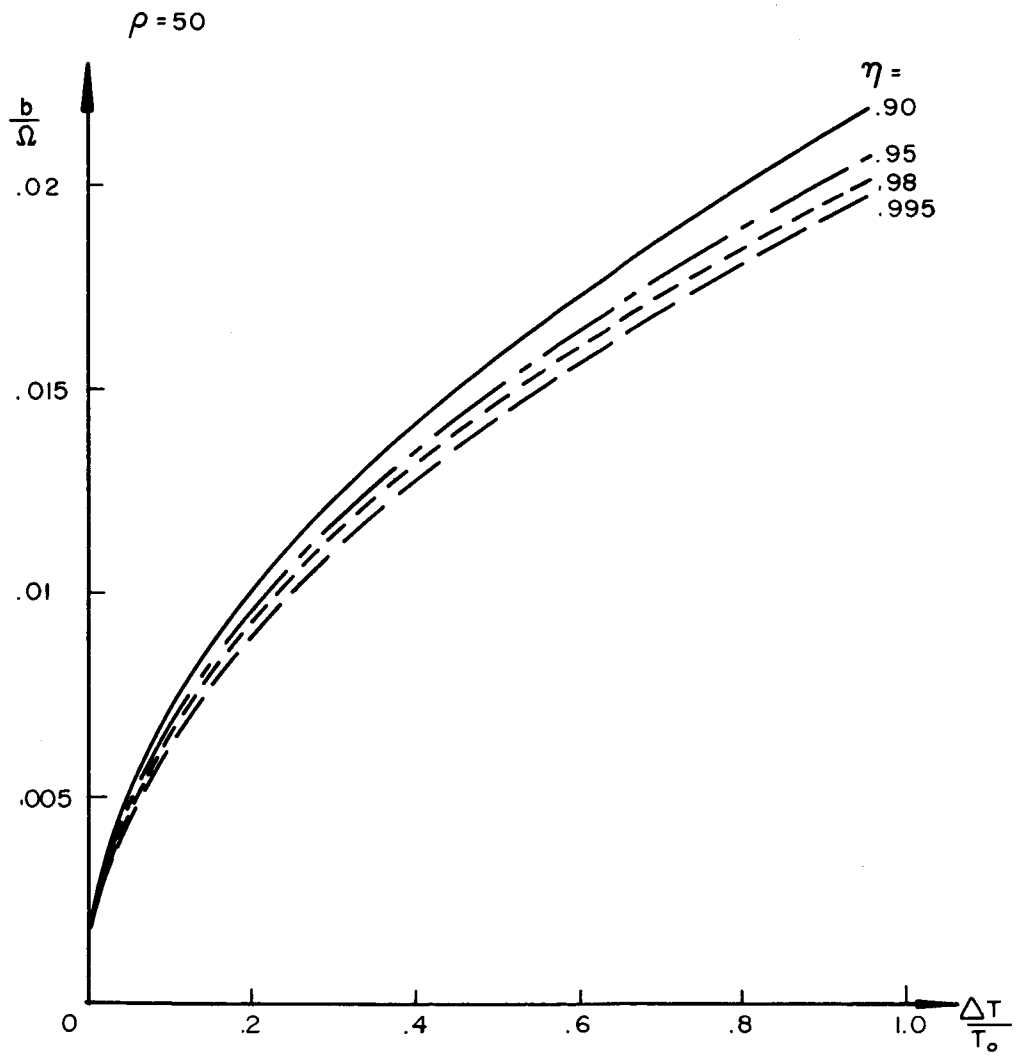

FIG. 5 AMPLITUDE TO TRUE SPIN RATIO OF THE ANGULAR VELOCITY ABOUT THE B AXIS VERSUS ENERGY DISSIPATION RATIO WITH THE UNSYMMETRY FACTOR AS PARAMETER

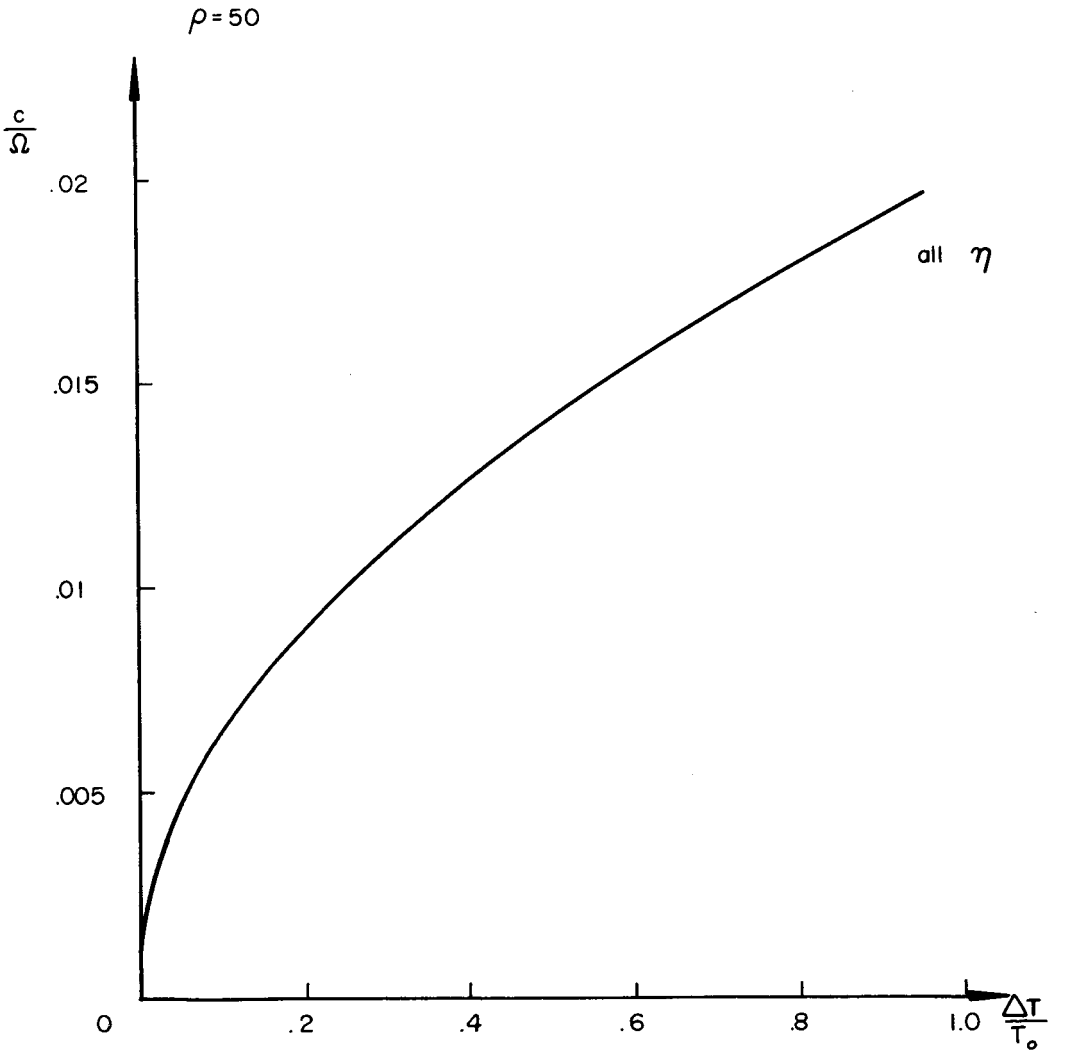

FIG. 6 AMPLITUDE TO TRUE SPIN RATIO OF ANGULAR VELOCITY ABOUT THE A AXIS VERSUS ENERGY DISSIPATION RATIO

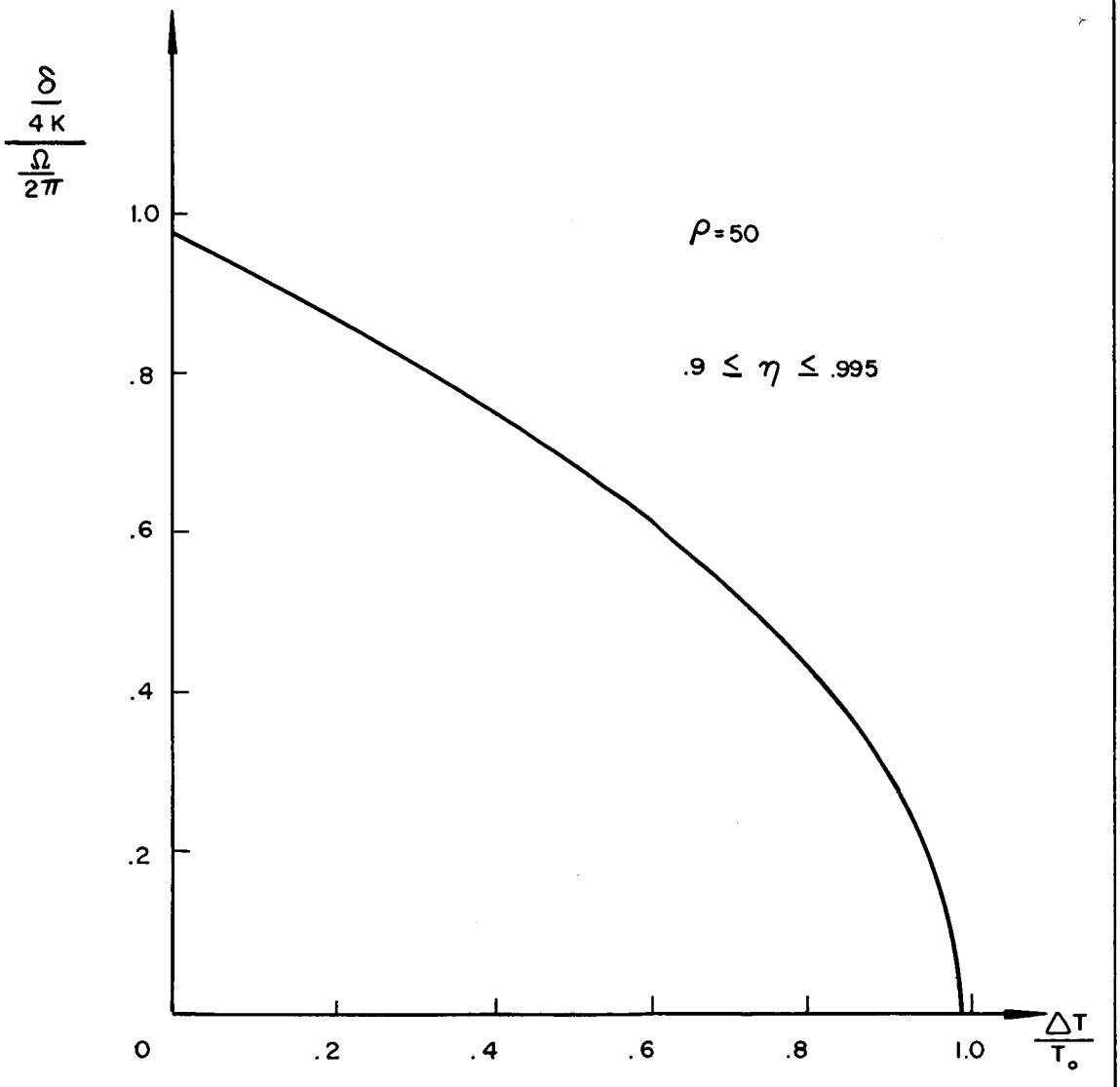

FIG. 7 FREQUENCY RATIO OF OSCILLATORY ANGULAR VELOCITIES TO THE INITIAL SPIN VELOCITY

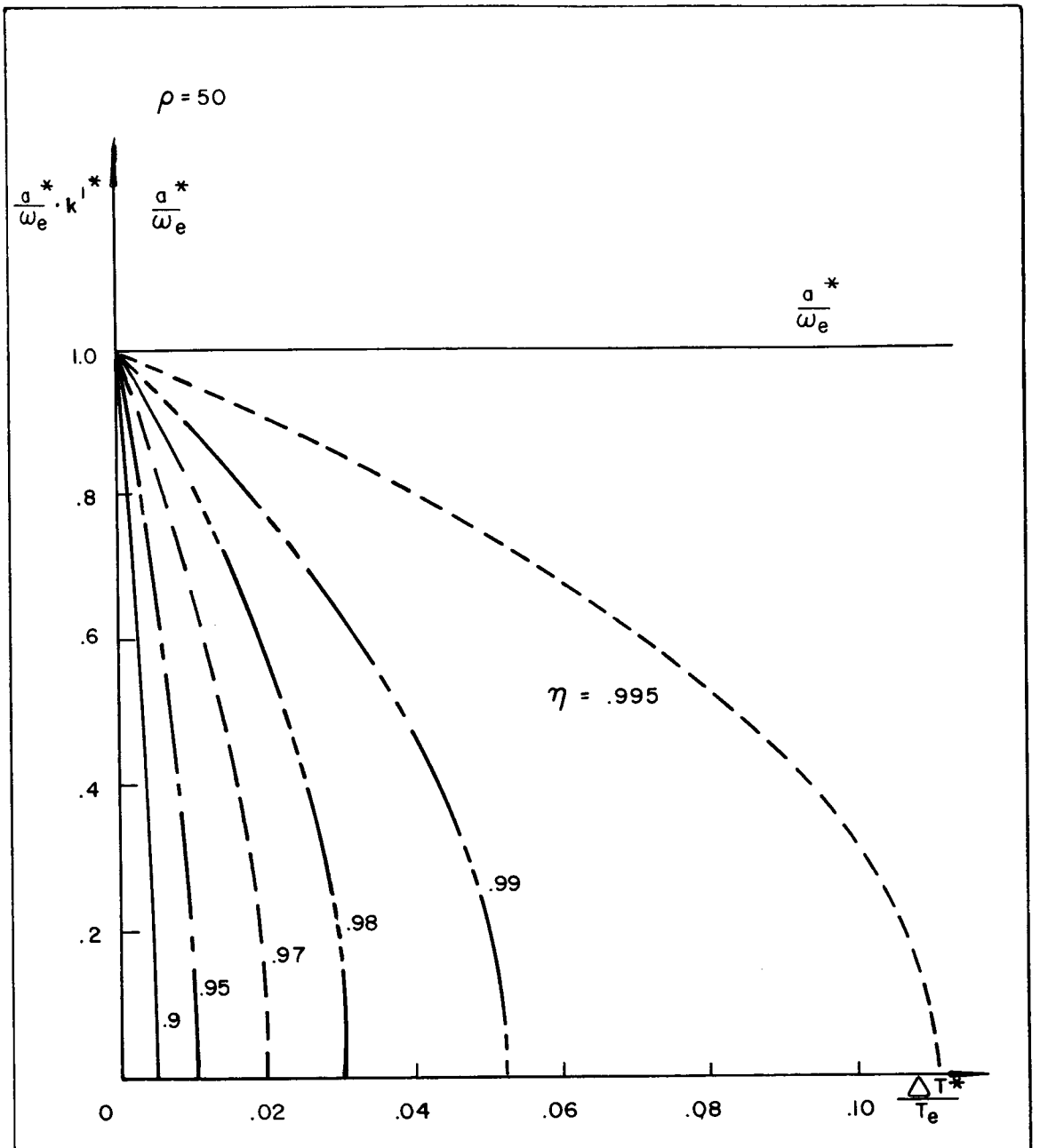

FIG. 8 AMPLITUDE TO FLAT SPIN RATIOS OF ANGULAR VELOCITY ABOUT THE A AXIS VERSUS ENERGY DISSIPATION RATIO WITH THE UNSYMMETRY FACTOR AS PARAMETER

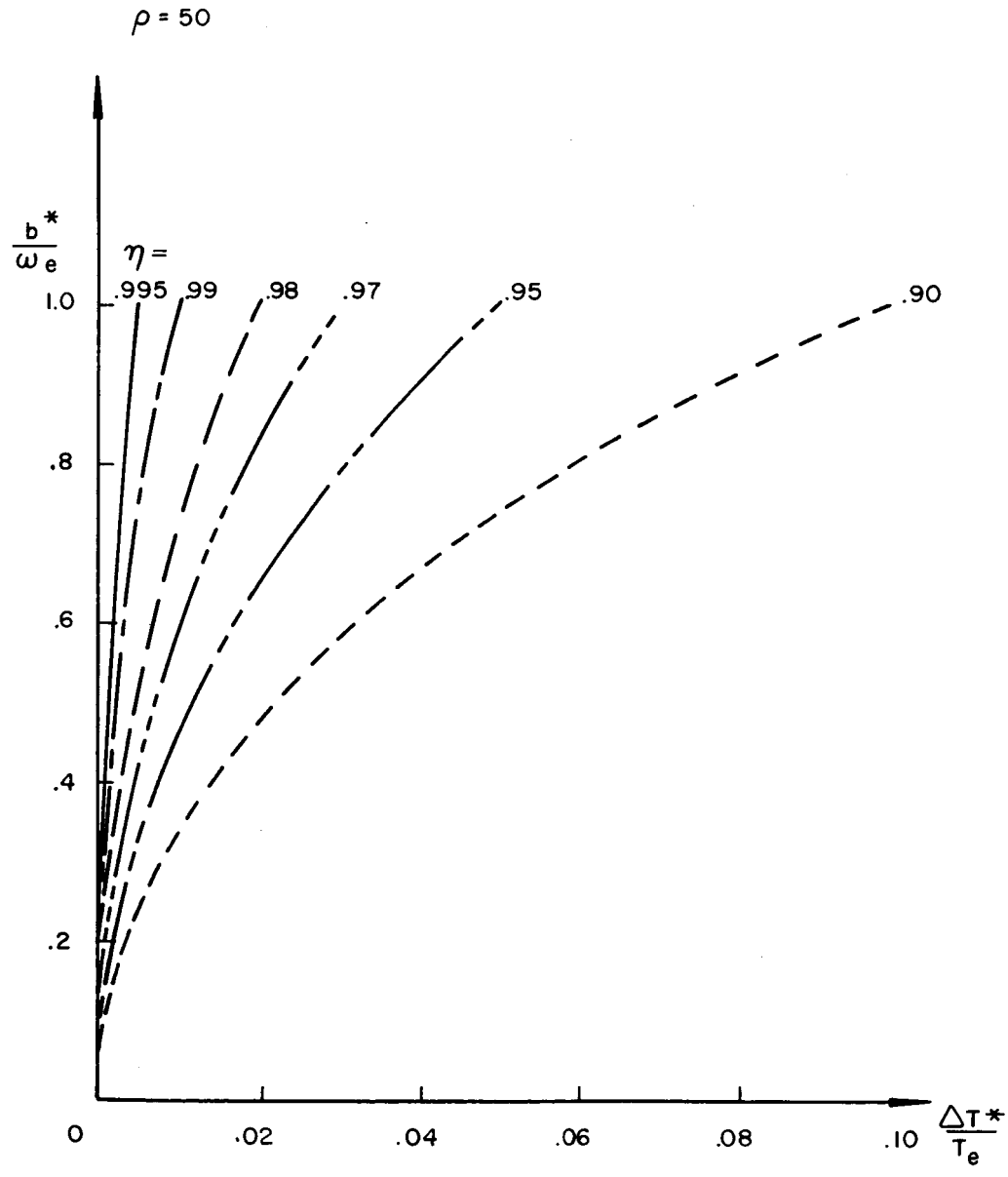

FIG. 9 AMPLITUDE TO FLAT SPIN RATIO OF ANGULAR VELOCITY ABOUT THE B AXIS VERSUS ENERGY DISSIPATION RATIO WITH THE UNSYMMETRY FACTOR AS PARAMETER

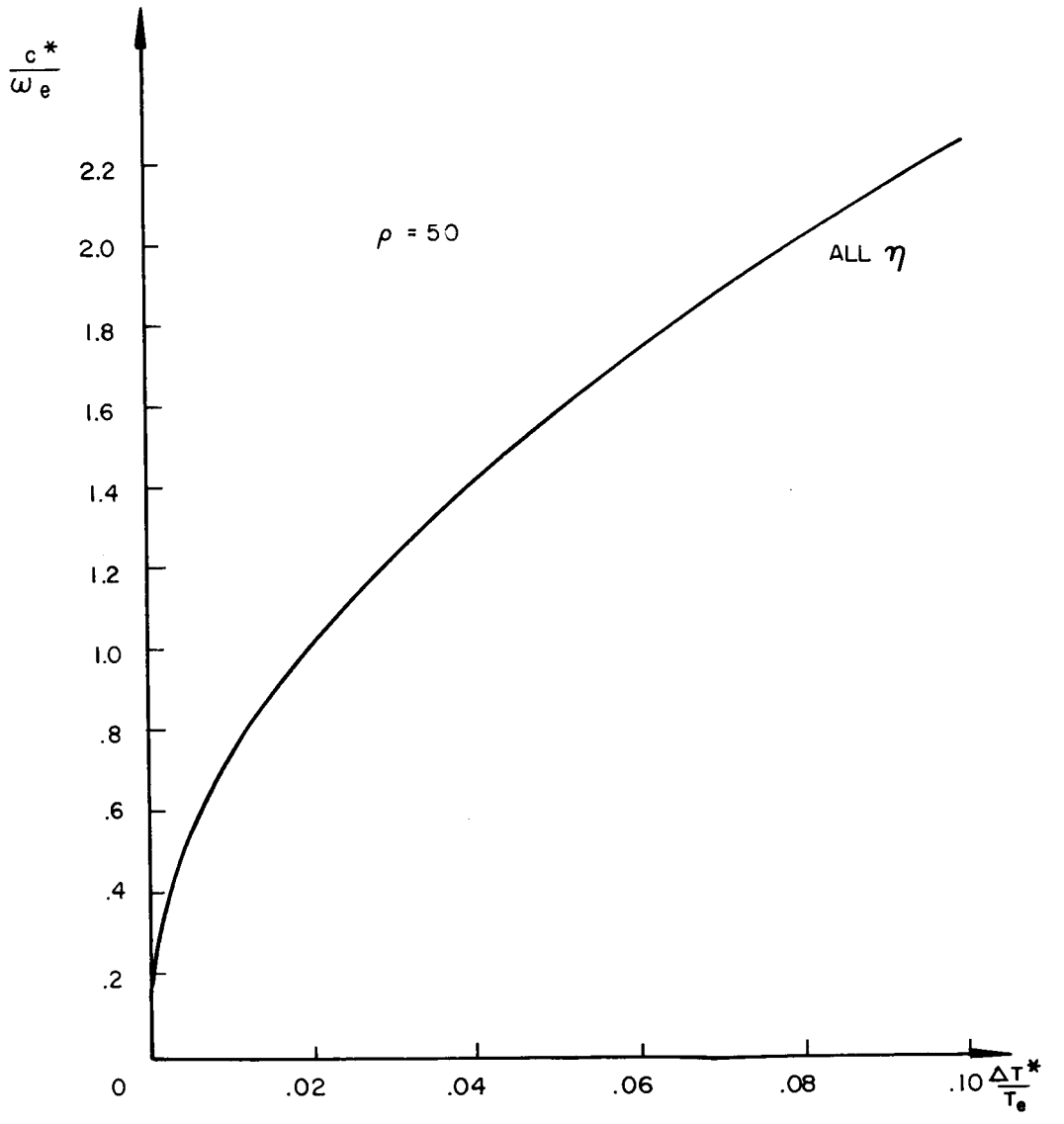

FIG. 10 AMPLITUDE TO FLAT SPIN RATIO OF ANGULAR VELOCITY ABOUT THE C AXIS VERSUS ENERGY DISSIPATION RATIO

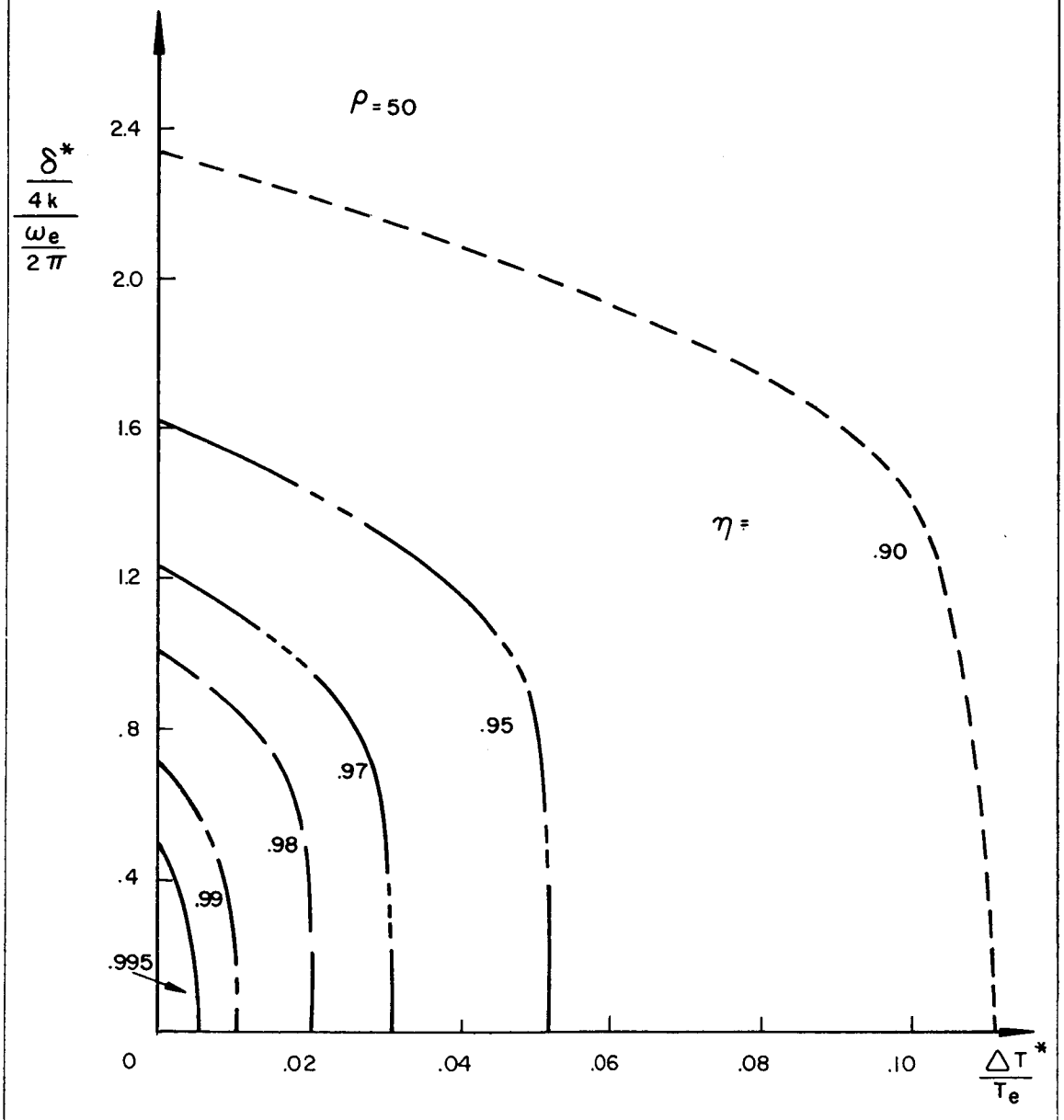

FIG. 11 RATIO OF THE FREQUENCY OF THE OSCILLATING ANGULAR VELOCITY TO THE FINAL FLAT SPIN RATE.

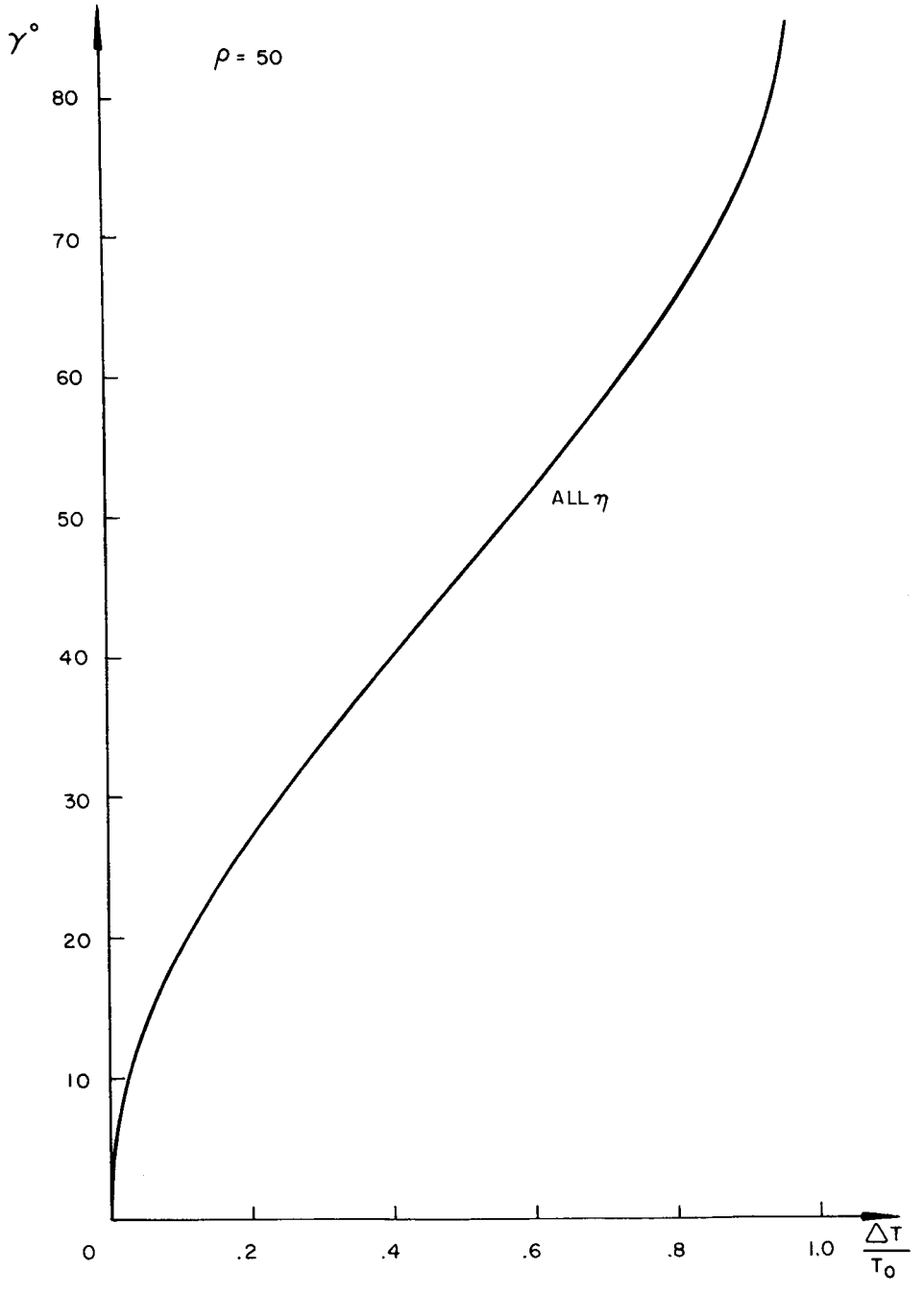

FIG. 12 ANGLE BETWEEN C AXIS AND ANGULAR MOMENTUM VECTOR AS FUNCTION OF THE ENERGY DISSIPATION RATIO.

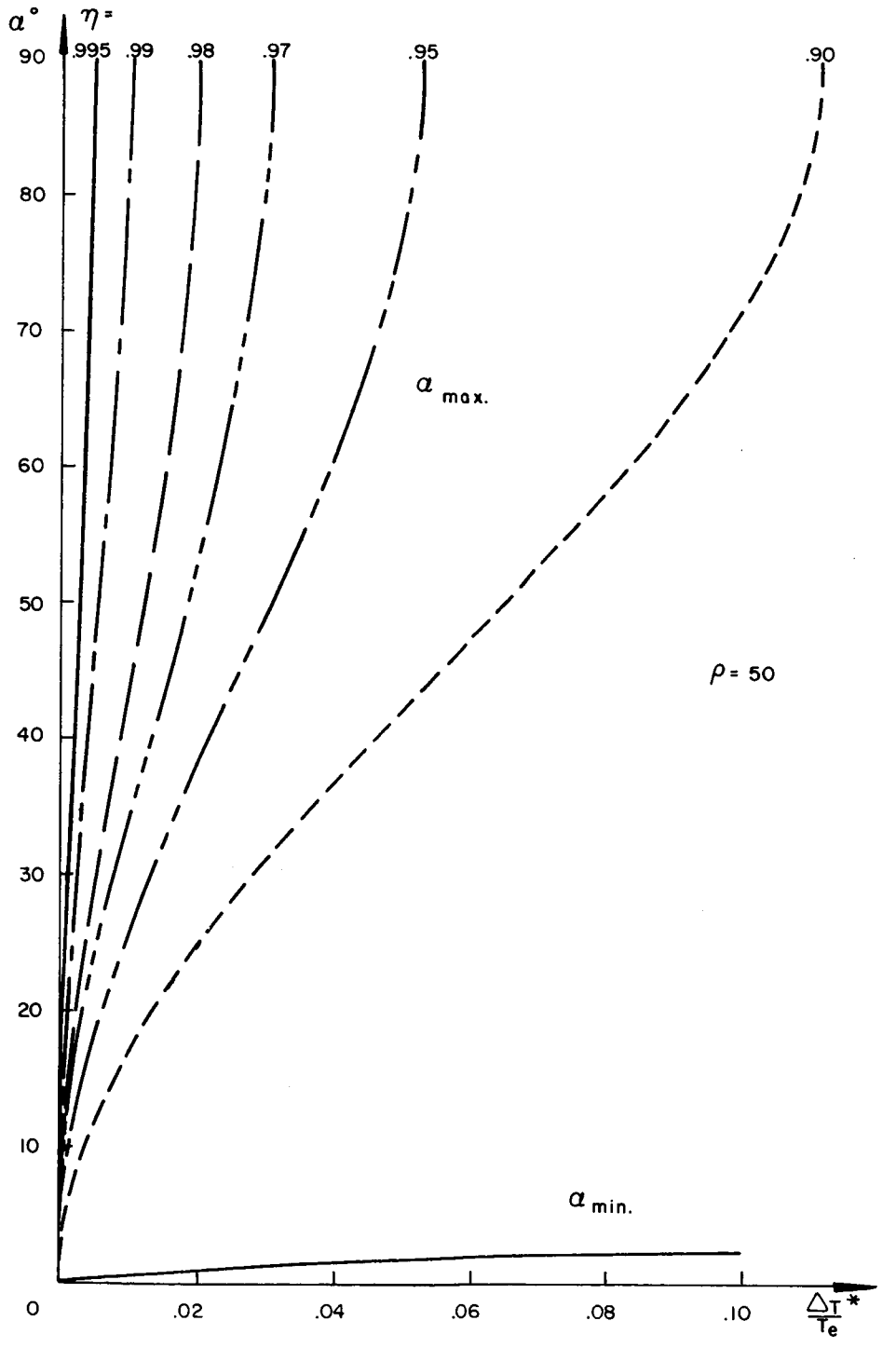

FIG. 13 MAXIMUM AND MINIMUM ANGLE BETWEEN A AXIS AND ANGULAR MOMENTUM VECTOR VERSUS ENERGY DISSIPATION RATIO WITH THE UNSYMMETRY FACTOR AS PARAMETER.

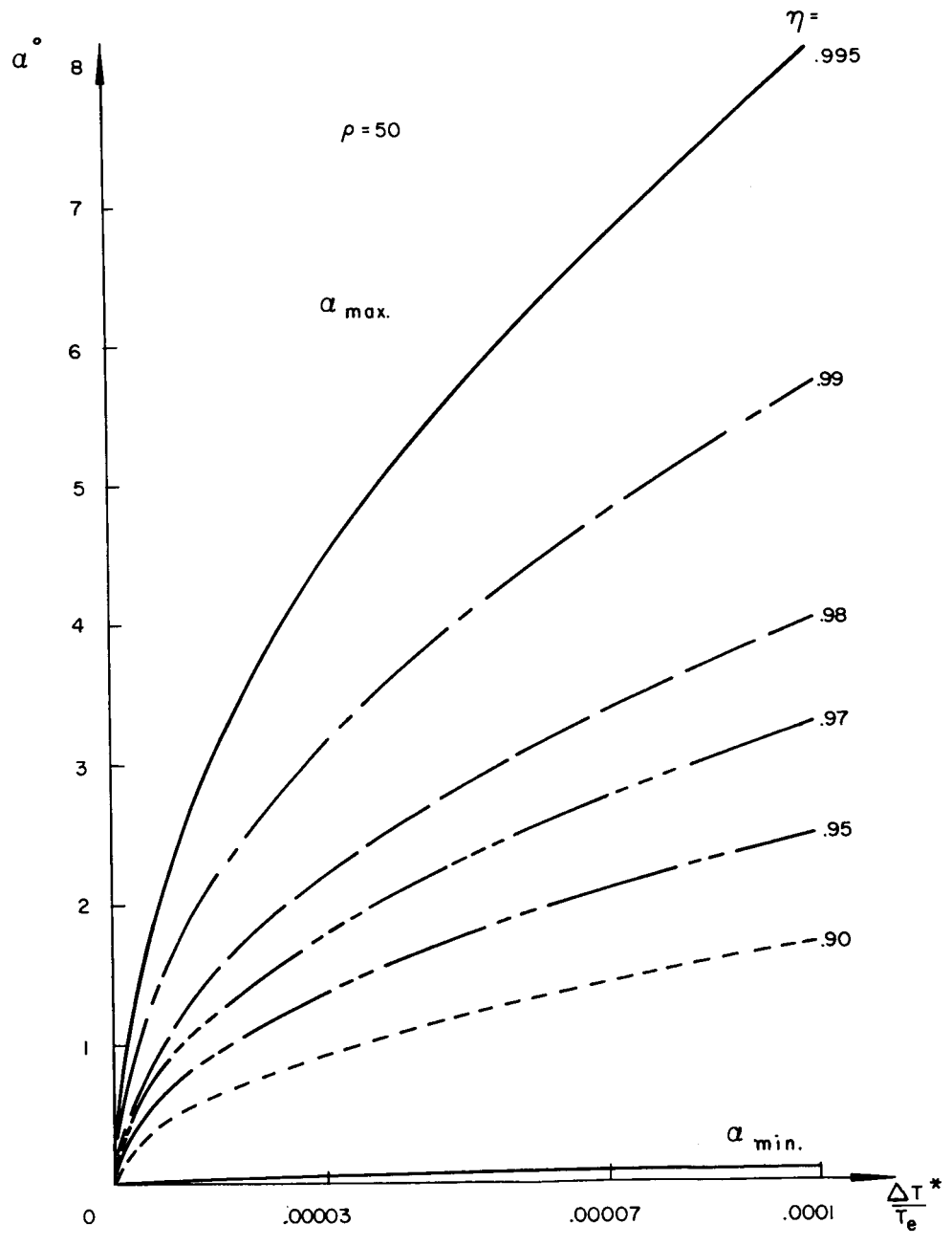

FIG. 13a MAXIMUM AND MINIMUM ANGLE BETWEEN A AXIS AND ANGULAR MOMENTUM VECTOR VERSUS ENERGY DISSIPATION RATIO WITH THE UNSYMMETRY FACTOR AS PARAMETER.

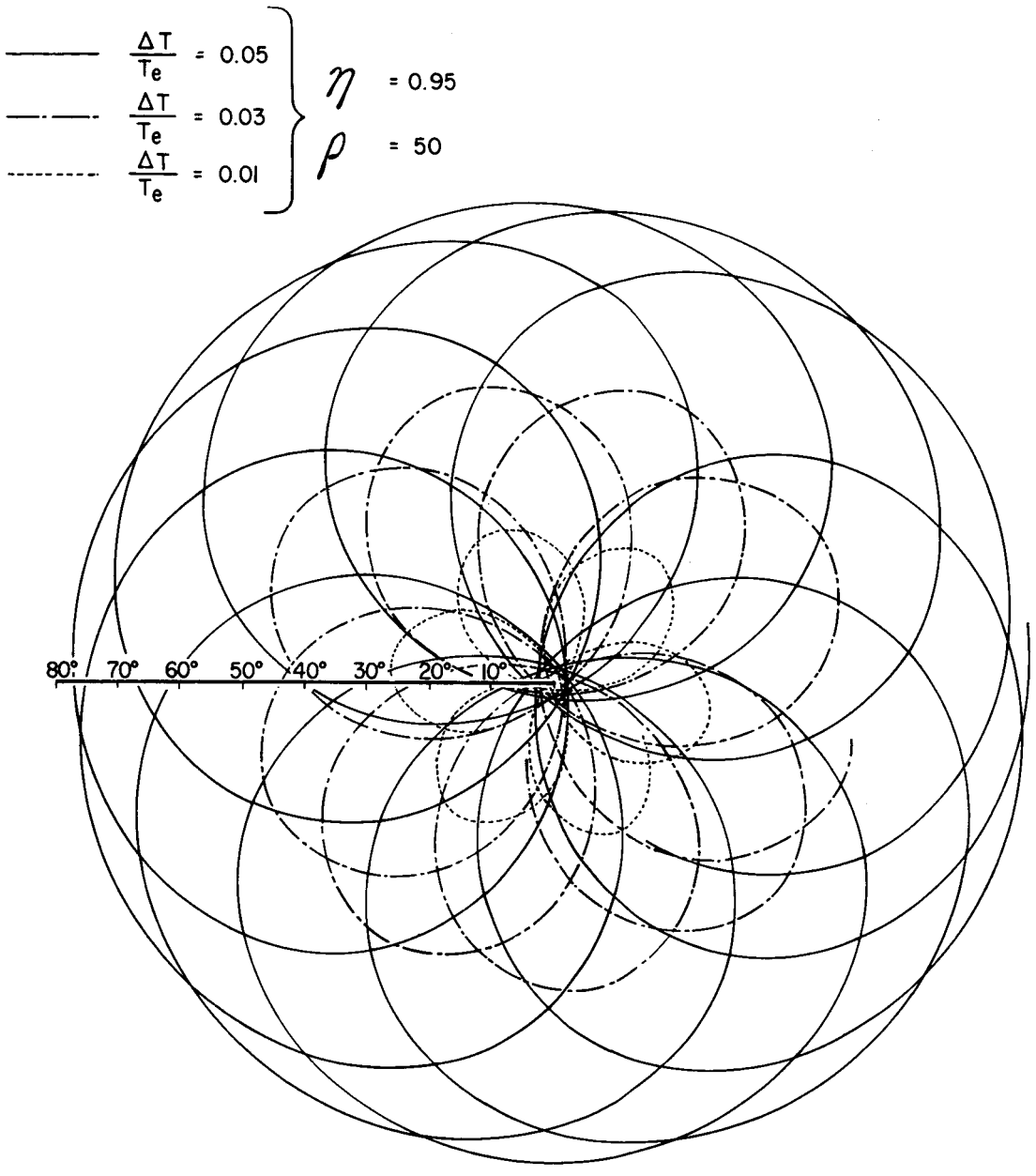

FIG 14 NUTATION AT APPROACH TO FLAT SPIN

PATH OF A POINT ON THE AXIS OF MAXIMUM MOMENT OF INERTIA AS SEEN FROM A SPACE FIXED OBSERVER LOOKING IN DIRECTION OF THE ANGULAR MOMENTUM VECTOR

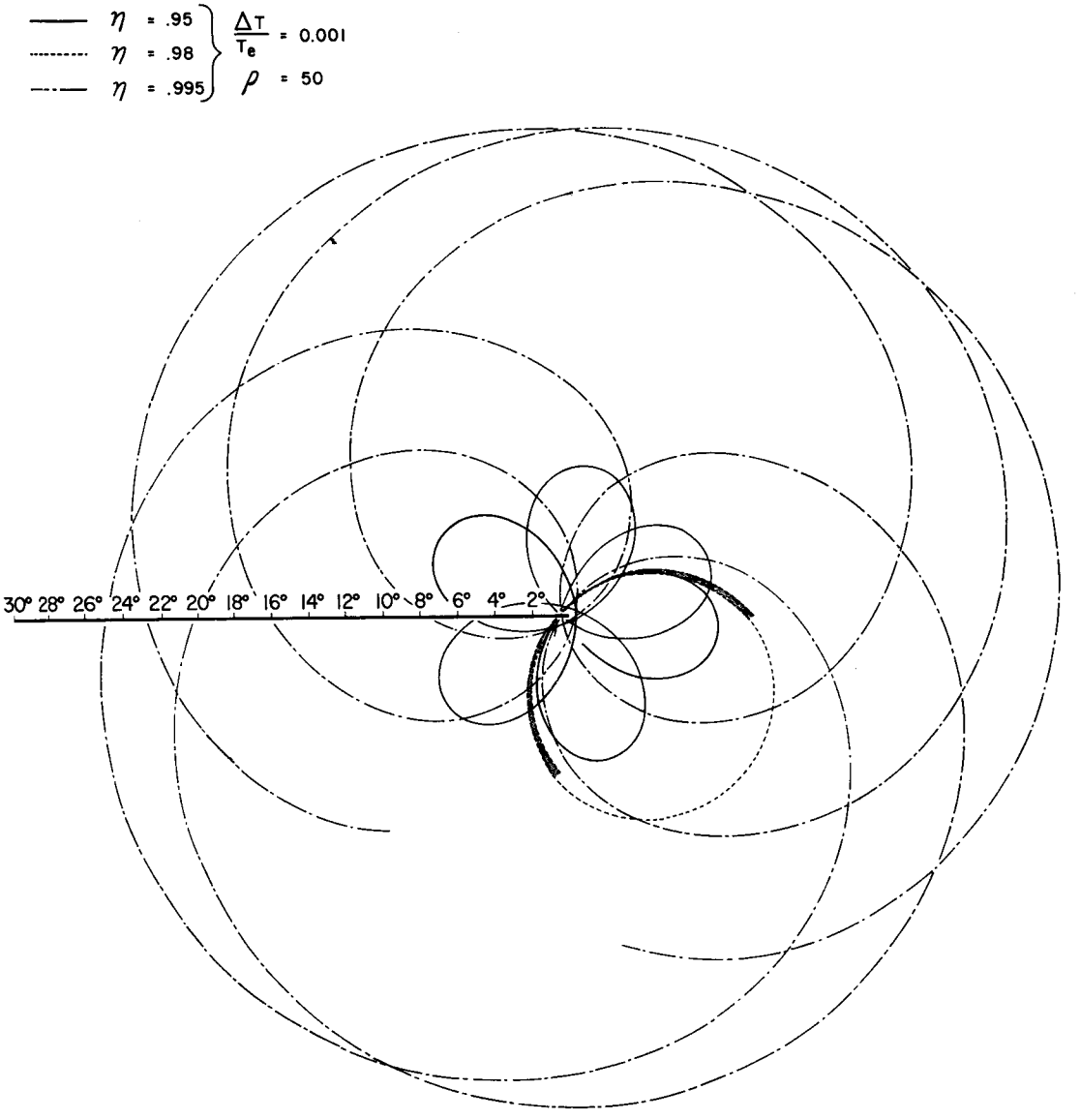

FIG 15 NUTATION AT APPROACH TO FLAT SPIN

PATH OF A POINT ON THE AXIS OF MAXIMUM MOMENT OF INERTIA AS SEEN FROM A SPACE FIXED OBSERVER LOOKING IN DIRECTION OF THE ANGULAR MOMENTUM VECTOR

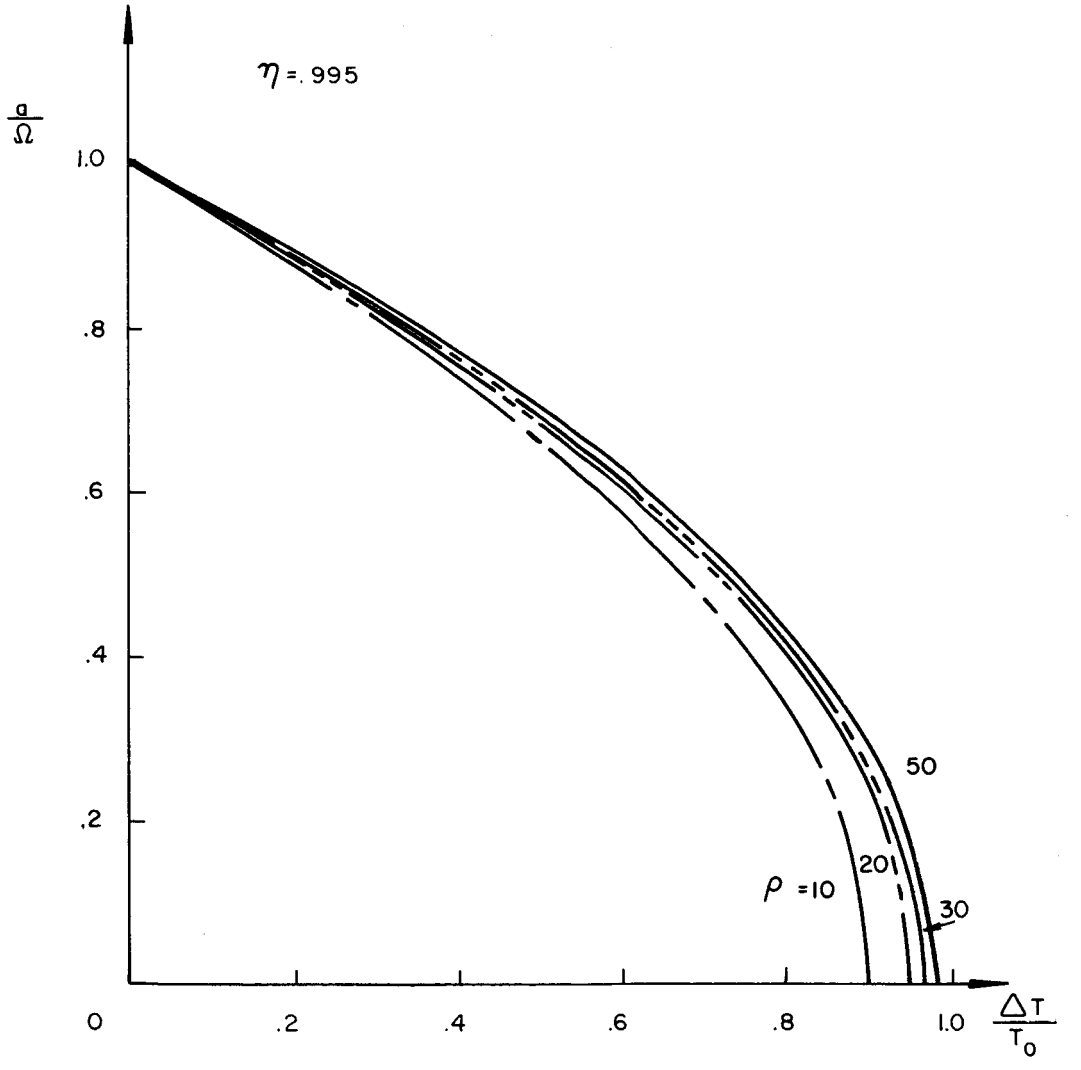

FIG.16 INFLUENCE OF THE ROD RATIO ON THE ANGULAR VELOCITY ABOUT THE C AXIS

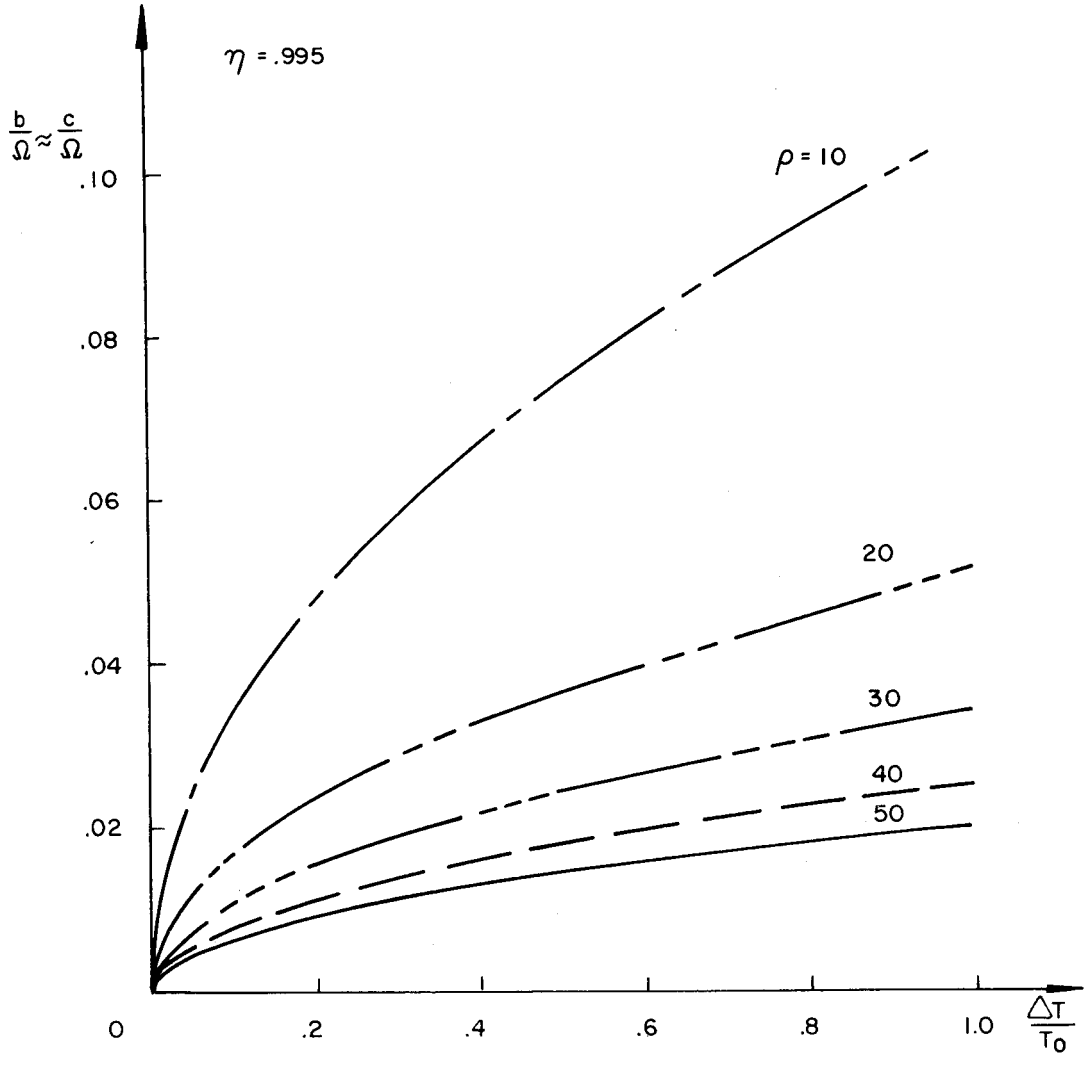

FIG. 17 INFLUENCE OF THE ROD RATIO ON THE ANGULAR VELOCITY ABOUT THE B AXIS

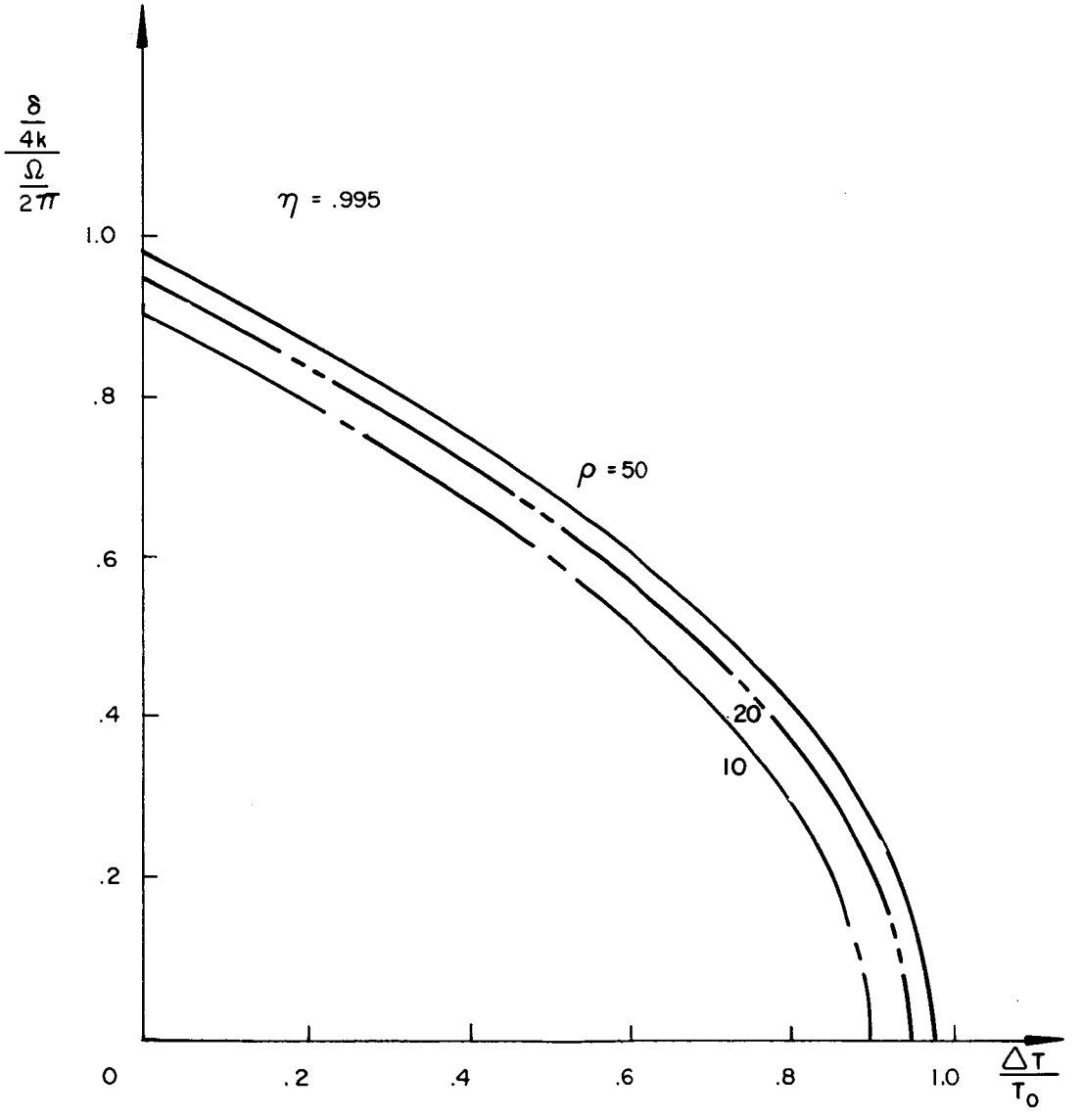

FIG. 18 INFLUENCE OF THE ROD RATIO ON THE FREQUENCY OF THE OSCILLATORY ANGULAR VELOCITIES

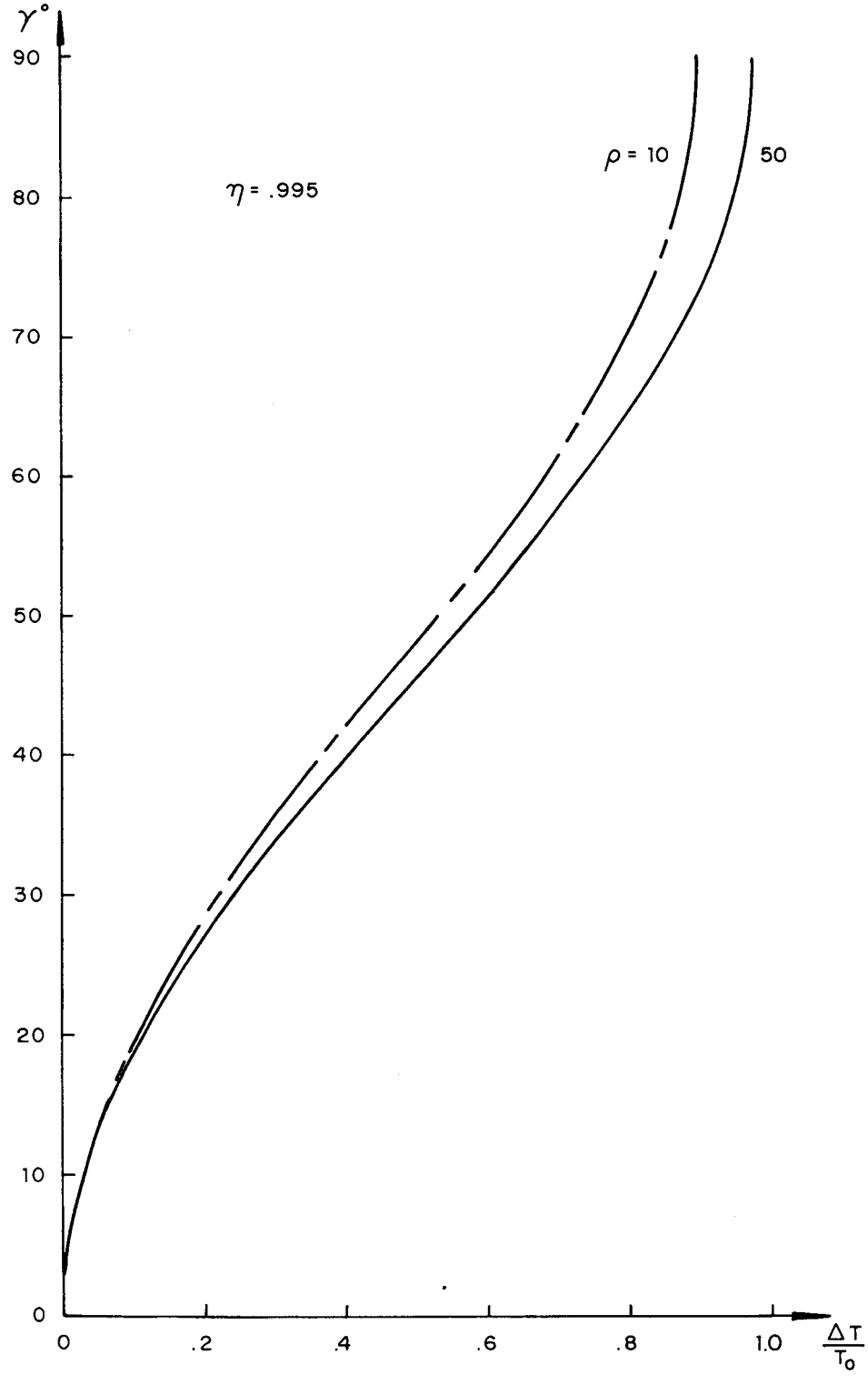

FIG. 19 - INFLUENCE OF THE ROD RATIO ON THE NUTATION ANGLE DESCRIBED BY THE C AXIS

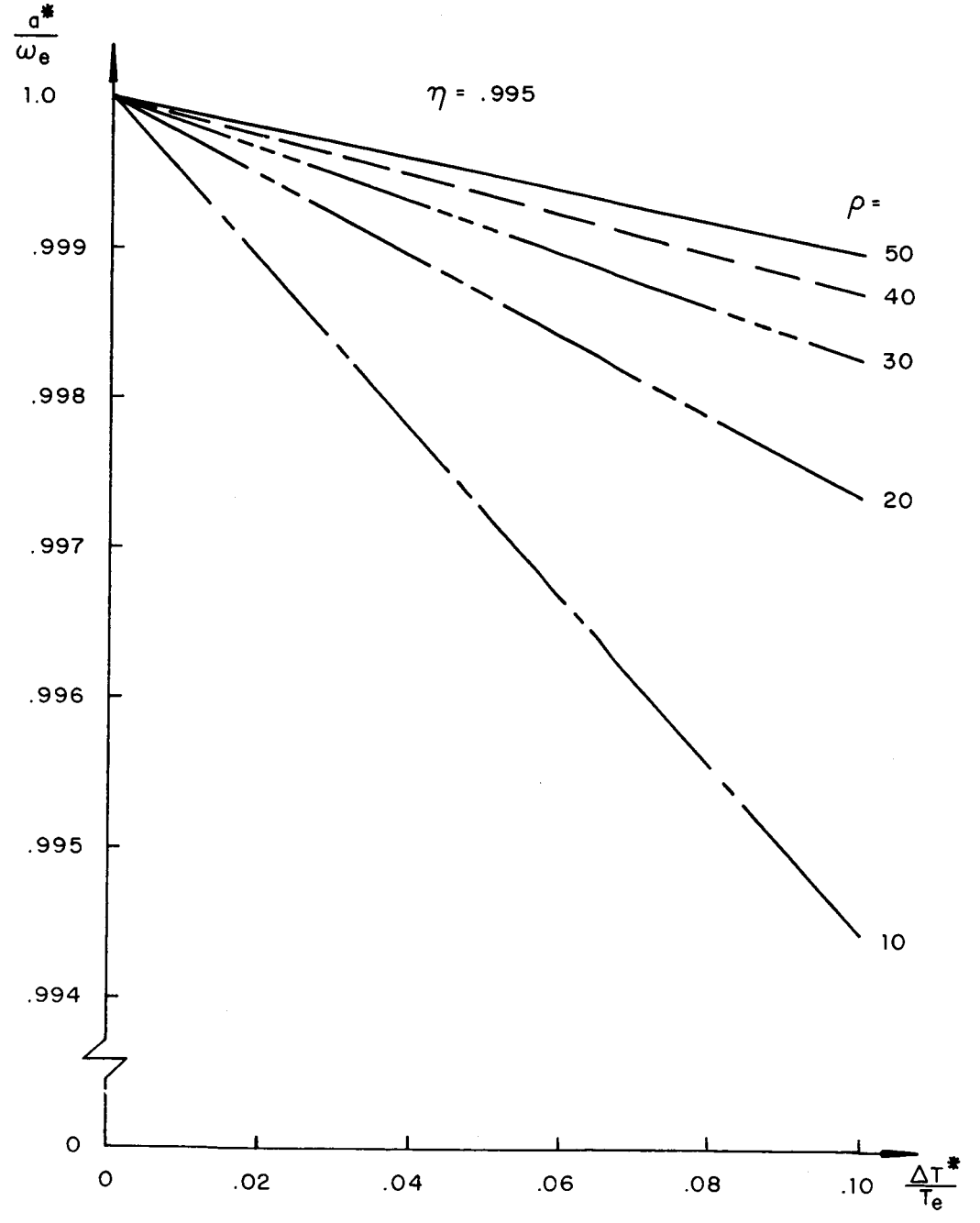

FIG. 20 - INFLUENCE OF THE ROD RATIO ON THE ANGULAR VELOCITY ABOUT THE A AXIS

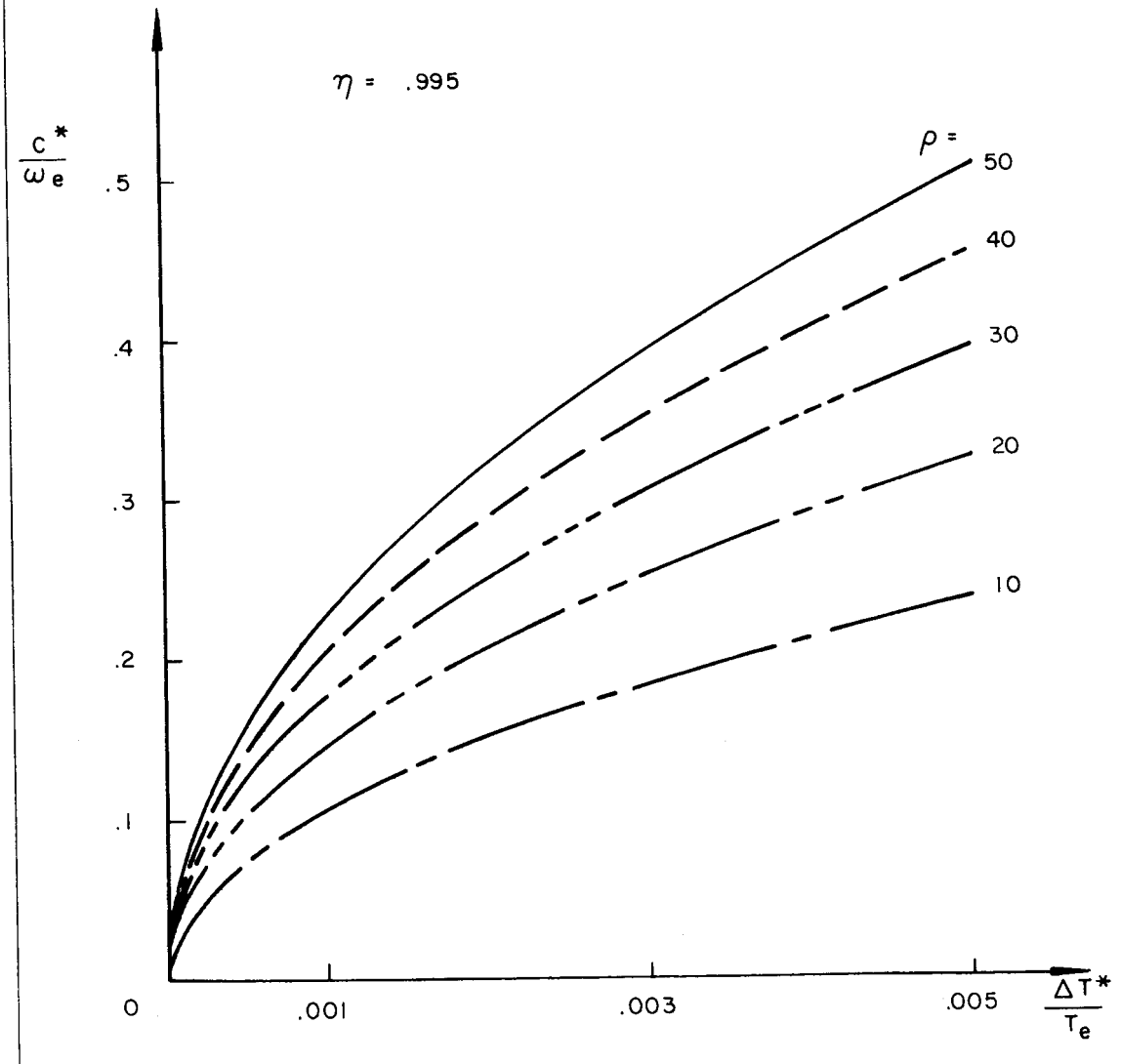

FIG. 21 INFLUENCE OF THE ROD RATIO ON THE ANGULAR VELOCITY ABOUT THE C AXIS

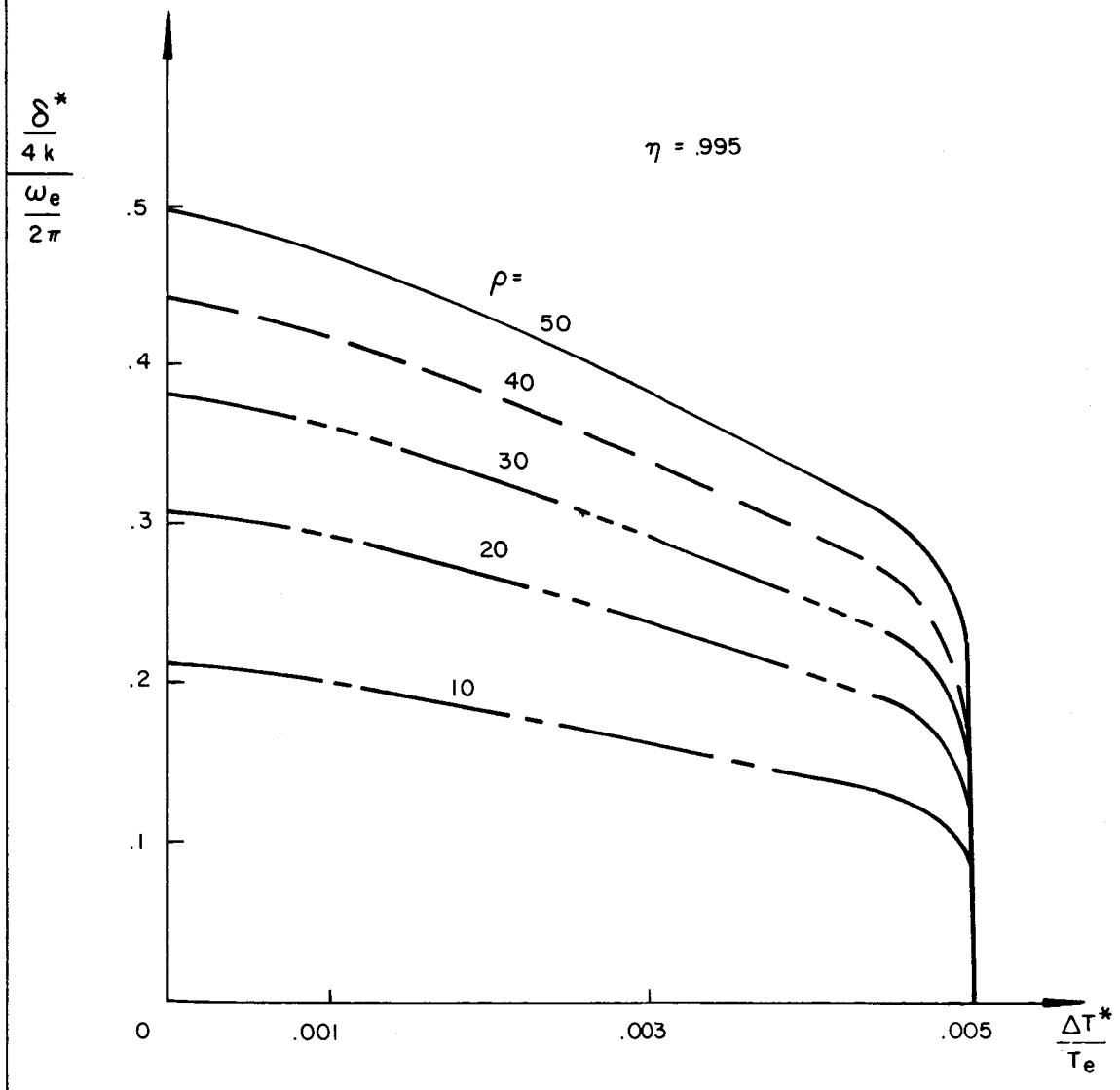

FIG. 22 INFLUENCE OF THE ROD RATIO ON THE FREQUENCY OF THE OSCILLATORY ANGULAR VELOCITIES

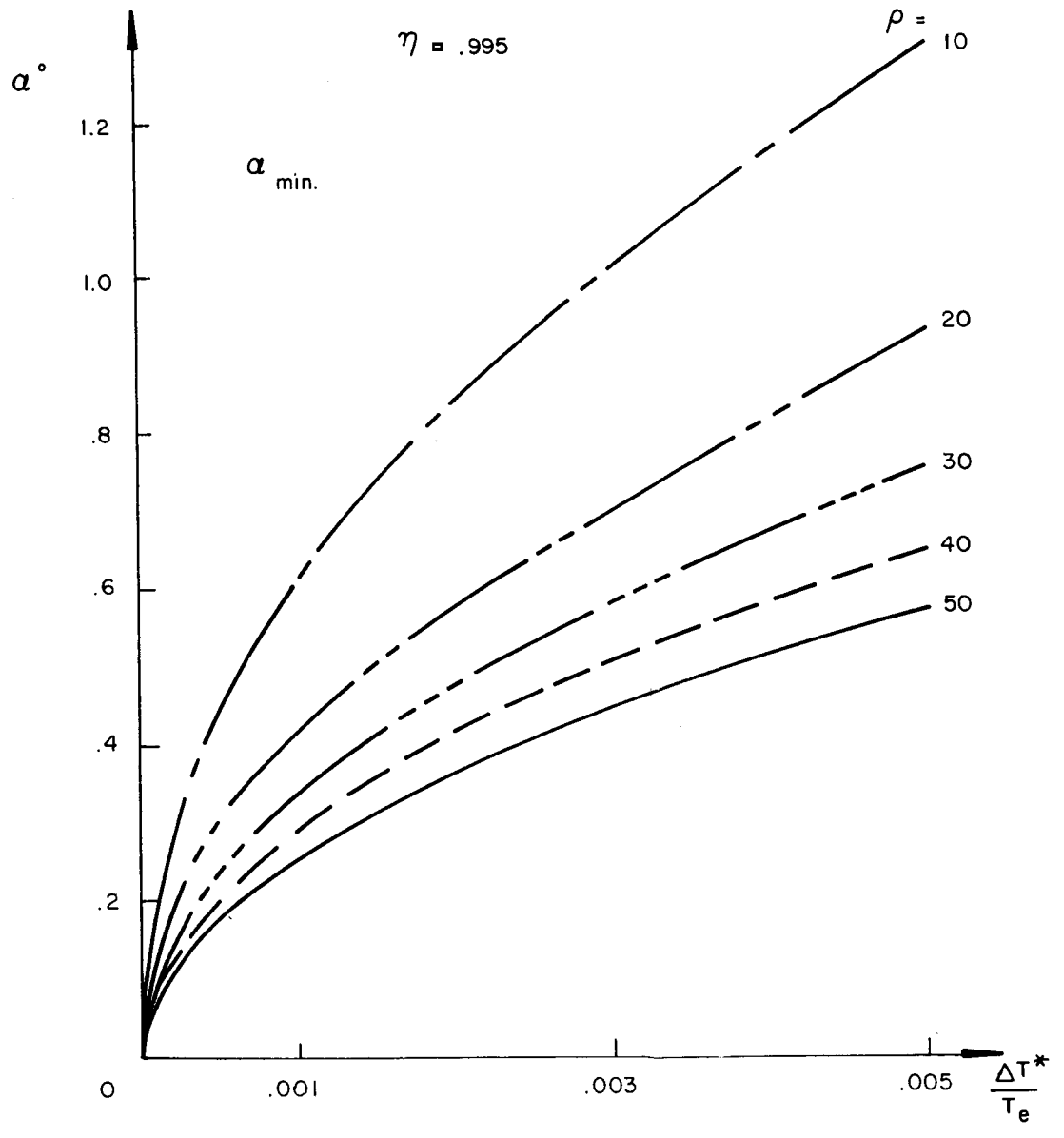

FIG. 23 INFLUENCE OF THE ROD RATIO ON THE NUTATION ANGLE DESCRIBED BY THE A AXIS